# NLTE Synthetic Spectral Fits to the Type Ia Supernova 1994D in NGC 4526

Eric J. Lentz[1], E. Baron, David Branch

*Department of Physics and Astronomy, University of Oklahoma, 440 W. Brooks St., Norman, OK 73019-0225*

and

Peter H. Hauschildt

*Department of Physics and Astronomy & Center for Simulational Physics, University of Georgia, Athens, GA 30602-2451*

## ABSTRACT

We have fit the normal, well observed, Type Ia Supernova (SN Ia) SN 1994D with non-LTE spectra of the deflagration model W7. We find that well before maximum luminosity W7 fits the optical spectra of SN 1994D. After maximum brightness the quality of the fits weakens as the spectrum forms in a core rich in iron peak elements. We show the basic structure of W7 is likely to be representative of the typical SN Ia. We have shown that like W7, the typical SN Ia has a layer of unburned C+O composition at $v > 15000$ km s$^{-1}$, followed by layers of C-burned and O-burned material with a density structure similar to W7. We present UVOIR (UBVRIJKH) synthetic photometry and colors and compare with observation. We have computed the distance to the host galaxy, NGC 4526, obtaining a distance modulus of $\mu = 30.8 \pm 0.3$. We discuss further application of this direct measurement of SNe Ia distances. We also discuss some simple modifications to W7 that could improve the quality of the fits to the observations.

*Subject headings:* galaxies: individual (NGC 4526) — stars: atmospheres — supernovae: individual (SN 1994D)

## 1. Introduction

Type Ia Supernovae (SNe Ia) have contributed to the chemical evolution of the universe by releasing iron peak and alpha chain elements into the various star forming and other gaseous regions. As SNe Ia are among the brightest objects known and their light curves can be used to improve their uniformity, they are among the most useful objects with which to study the structure and

[1]Present address: Department of Physics and Astronomy & Center for Simulational Physics, University of Georgia, Athens, GA 30602

nature of the universe (Riess et al. 1998; Perlmutter et al. 1999). It is therefore important to have a fuller understanding of the underlying physics and origin of SNe Ia.

The current understanding of the progenitor system for SNe Ia features a sub-Chandrasekhar mass C+O white dwarf accreting mass from an ordinary star until reaching the Chandrasekhar mass, or by merging with another C+O white dwarf and then exploding (**?**, cf.)and references therein]prog95,livio99. SNe Ia scenarios with sub-Chandrasekhar mass explosions have not been able to reproduce the observed spectra and photometry (Nugent et al. 1997; Höflich et al. 1997).

SN 1994D, in NGC 4526, was discovered 2 weeks before maximum brightness (Treffers et al. 1994). It was one of the best observed SNe Ia, with near-daily spectra starting 12 days before maximum brightness (-12 days) and continuing throughout the photospheric phase. SN 1994D has been well observed photometrically (Richmond et al. 1995; Patat et al. 1996; Meikle et al. 1996; Tsvetkov & Pavlyuk 1995) and spectroscopically (Filippenko 1997; Patat et al. 1996; Meikle et al. 1996). Wang et al. (1997) found no significant polarization in SN 1994D 10 days before maximum light. Cumming et al. (1996) placed a limit on a solar-composition progenitor wind of $1.5 \times 10^{-5}$ $M_\odot$ $yr^{-1}$ for a 10 km $s^{-1}$ wind. SN 1994D has been previously modeled with synthetic spectra and light curves by several groups (Hatano et al. 1999; Höflich 1995; Meikle et al. 1996; Mazzali & Lucy 1998). Our goal in this paper is to take a large set of observed spectra and a detailed (even if somewhat parameterized) hydrodynamical model and confront the two. Höflich (1995) did this to some extent, but focused on the photometry more heavily, partly because much of the spectroscopy has

SNe Ia with spectral coverage this frequent and early are still quite rare. Other SNe Ia with excellent spectral coverage are: SN 1989B (Wells et al. 1994), discovered approximately 7 days before maximum light, SN 1996X (Salvo et al. 2001), discovered 6 days before maximum light, and SN 1998bu (Jha et al. 1999; Hernandez et al. 2000), discovered 10 days before maximum light. Both of these well observed, normal SNe Ia were discovered after the phase in SN 1994D when daily spectral coverage had already begun. This aspect of the available data for SN 1994D make it still the best candidate for detailed, multi-epoch spectrum synthesis of the photospheric phase, especially at the earliest dates. This detailed and early set of spectra allow us to probe the spectrum formation at early epochs, and therefore the outermost layers of the supernova.

## 2. Numerical Technique

We have used the multi-purpose spectrum synthesis and model atmosphere code `PHOENIX 9.1` (**?**, see)and references therein]hbjcam99. `PHOENIX` has been designed to accurately include the various effects of special relativity important in rapidly expanding atmospheres, like supernovae. Ionization by non-thermal electrons from $\gamma$-rays from the nuclear decay of $^{56}$Ni that powers the light curves of SNe Ia is taken into account. We have tested, in a few models, an updated method for calculating the $\gamma$-ray deposition using a solution of the spherically symmetric radiative transfer

equation for $\gamma$-rays with PHOENIX, and found no difference in deposition or temperature convergence relative to the older, single $\Lambda$-iteration technique of Nugent (1997) which is based on the method of Sutherland & Wheeler (1984). We used an effective $\gamma$-ray opacity, $\kappa_\gamma = 0.06$ $Y_e$ cm$^2$ gm$^{-1}$ (Colgate et al. 1980) for all calculations. In the models presented here we solve the NLTE rate equations for H I (10 levels/37 transitions), He I (19/37), He II(10/45), C I (228/1387), O I (36/66), Ne I (26/37), Na I (3/2), Mg II (73/340), Si II (93/436), S II (84/444), Ti II (204/2399), Fe II (617/13675), and Co II (255/2725), which we have chosen both for computational efficiency and to be consistent with what was used in our earlier work (Nugent et al. 1997, 1995). In future work we will use more species in NLTE, but test calculations show that this is the primary feature forming species of each element and that it set is quite adequate.

The model W7 was prepared by homologous expansion using a rise time of 20 days after explosion to maximum light (**?**, e.g.,)]riessetalIaev00,akn00. The hydrodynamic output was extended from $\sim$ 24000 km s$^{-1}$ to 30000 km s$^{-1}$ with the unburned C+O white dwarf composition as in previous PHOENIX calculations using W7 (Nugent et al. 1997; Nugent 1997; Lentz et al. 2000). At each epoch, we have fit the luminosity to match the shape and color of the observations, while solving for the energy balance and converged NLTE rate equations. To fit the spectra, after having fixed the date of explosion (20 days before maximum brightness in B), the model (W7), and the NLTE species, the only parameter we allow to vary is the bolometric luminosity of the model. The bolometric luminosity for a model with a fixed density structure is a required boundary condition for the system of equations, but it may also be convienently thought of in terms of a "model temperature" so that one can see that varying the model temperature is the degree of freedom necessary to match of the shape of the synthetic spectrum to the observations. We have found that with luminosity changes of less than 20% it is difficult to discern differences in the quality of the fit, except in certain cases with good observed spectral coverage and good synthetic spectral fits. This corresponds to about 5% differences in temperature and about 0.2 magnitudes in the absolute luminosity calibration. Our selection of the best fit is done by eye and at least two of the authors independently select the best fit. While a lot of experience is involved in selecting the best fit, we first strive to fit the overall shape (or colors) and then we strive to fit the lineshape of selected lines. We are developing statistical tests to improve the sensitivity and we note that we are sensitive to much smaller variations of order 0.02 mag when this method is applied to SNe II (R. Mitchell et al., E. Baron et al., in preparation).

## 3. Synthetic Spectra

We have calculated synthetic spectra from -12 days after maximum light (day 8 after explosion) to 12 days after maximum light (day 32 after explosion). The plotted synthetic spectra have been multiplied by an arbitrary constant to give the best fit to the de-redshifted and de-reddened observation. We have adopted the reddening, $E(B-V) = 0.06$, of Patat et al. (1996). The quoted error, $\pm 0.02$, is consistent with the other estimates of $E(B-V)$ (**?**, cf.)]DR94D99. Using $E(B-$

$V) = 0.06$, we have applied the Cardelli et al. (1989) reddening law to deredden the observations for comparison with the synthetic spectra. We have de-redshifted the observed spectra by $v = 830$ km s$^{-1}$ (Cumming et al. 1996) for the heliocentric velocity of the supernova, which is at the 0.3 % level. Synthetic optical and infra-red photometry are listed in Table 1. Observed colors and reddened synthetic colors are listed in Table 2 for comparison.

### 3.1. Before Visual Maximum

#### *3.1.1. 9 March 1994*

We plot the 9 March 1994 observed spectrum of SN 1994D with our best synthetic spectrum at day 8 after the explosion in Figure 1. The features of the synthetic spectrum match the observations in strength and shape, except the large Ca II H+K absorption at 3800 Å. This feature is not well produced in the earliest synthetic spectra due to over-ionization, which we discuss in § 5.3. The 6000 Å Si II absorption is shifted upward somewhat by a small difference in the 'continuum' between the model and SN 1994D, but the strength and shape are otherwise fine. Of special note is the broad Fe II feature at 4500–5000 Å. Hatano et al. (1999) attribute this feature to high-velocity iron in the unburned, or at least unenhanced by fresh iron, layers of the supernova. We concur with this conclusion, and note that if any minima exist in the Fe II opacity, as they needed to fit the shape the feature, the minima arise naturally from the radiative equilibrium and NLTE treatment within the W7 model. The red minimum in the absorption is weaker in our fit than in the observation, but the two minima are clearly indicated. This feature is robust. In a model with one-half the luminosity, the Fe II feature remains strong and continues to form in high-velocity material, though the total flux blueward of that feature (synthetic spectrum not plotted) is greatly reduced relative to the red flux. We have also tested the Fe II hypothesis. In a spectrum containing only Fe II line opacity the feature appeared with the same shape and strength. This technique is discussed in § 5.1.

The overall shape of the synthetic spectrum fits the peaks in the spectrum as well as the 'continuum' flux level blue of the Ca II H+K feature and red of the Si II feature. The $B-V$ and $V-R$ colors are within 0.1 mag of the observed values, which is less than the estimated errors, and therefore in agreement. The weakness of the Ca II H+K feature in the synthetic spectrum decreases (brightens) $M_U$ by about 0.2 magnitudes.

#### *3.1.2. 10 March 1994*

We plot the 10 March 1994 observed spectrum of SN 1994D with our best synthetic spectrum at day 9 in Figure 2. The 'continuum' levels and spectral features of the synthetic again match the observation except for the Ca II H+K absorption. The features are similar to the 9 March spectrum

and the day 8 synthetic spectrum, including the deep, fast Fe II feature. The colors are consistent with observations except $U-B$, which is too small, clearly caused by the weak Ca II H+K feature in the synthetic spectrum.

### *3.1.3. 11 March 1994*

We plot the 11 March 1994 observed spectrum of SN 1994D with our best synthetic spectrum at day 10 in Figure 3. Note that the observations obtained by Patat are in cgs, whereas those obtained at Lick are in arbitrary units. Both scales are linear, so the reader should be able to judge the fit quality equally well when comparing between spectra obtained by different observers. Again the model and observation are quite similar to the previous two dates. However, the Fe II feature is changing in shape and is no longer as strong. This is reflected in the synthetic spectrum. The synthetic spectrum again falls short of the peak of the observed flux near 4000 Å, but this would be compensated if the Ca II H+K feature were stronger. This model has been chosen for the fit to the strength and shape of the Si II features and our estimate of the flux from the previous observations blueward of the Ca II H+K feature. The synthetic and observed optical colors are consistent. A good fraction of the 0.4 mag difference in the $U-B$ colors is related to the weak Ca II H+K feature.

### *3.1.4. 12 March 1994*

The 12 March 1994 observed spectrum of SN 1994D and our best synthetic spectrum at day 11 are displayed in Figure 4. Most of the features in the synthetic spectrum fit quite well at this epoch. The Ca II H+K feature is still weaker than the observed, but the relative strength has improved over the previous day. This is reflected in the better match of the $U-B$ synthetic color to the two observations. The fact that the model is bluer than the observations to the red of 6000 Å is likely due to the fact that there is not enough line blanketing produced by W7, (which would push flux from the blue to the red). We shall see that this is likely due to a flaw in the density and/or composition structure of the inner parts of W7. The remaining colors are consistent with observations.

### *3.1.5. 13 March 1994*

Figure 5 shows the 13 March 1994 observed spectrum of SN 1994D with our best synthetic spectrum at day 12. The synthetic spectrum fits the observation very well, with nearly all features represented, although some strengths are incorrect. The Ca II H+K feature is still weaker than the observation, but it now shows the 'split' which we have previously shown to be generated by a blend of Ca II H+K and Si II $\lambda$ 3858 (Nugent et al. 1997; Lentz et al. 2000). The blue Si II feature at 5800 Å is stronger than in the observation. Nugent et al. (1997) have shown that the relative

strength of the two features are an effective temperature diagnostic. The stronger blue Si II feature in the model indicates that the Si II line-forming region is cooler in the model than in SN 1994D. We can improve the ratio of the two Si II features by increasing the luminosity and therefore the temperature of the model, but this would change the overall shape of the spectrum. The flux levels in the red, and blue of the Ca II H+K feature, would not both match the observation. The part of the spectrum just blueward of Ca II H+K is a very sensitive temperature/luminosity diagnostic. The photometric colors of the synthetic spectrum and observations are consistent.

#### *3.1.6. 15 March 1994*

The SN 1994D observed spectrum of day 14 (15 March 1994) with our best synthetic spectrum is shown in Figure 6. The fit to the shape and features is good. The colors are in agreement, except $R-I$, which is bluer than the observations. This is the result of a modest red deficit redward of the Si II features. In order to estimate the accuracy of our parameter determination, we display the best fit model and observation with the models with luminosities $\pm 7\%$ from the best fit in Figure 7. The differences are largest around the Ca II H+K feature. This shows how accurately the fits can be made if spectra are available extending blueward of the Ca II H+K feature and the input model provides a well fit spectrum.

#### *3.1.7. 16 March 1994*

We plot the 16 March 1994 observed spectrum of SN 1994D with our best synthetic spectrum at day 15 in Figure 8. The fit has a good shape and many of the features fit. The Ca II H+K feature does not absorb blueward enough, and the feature just blueward absorbs much too strongly. The synthetic colors are good, especially the $U-B$ which agrees very well with Patat et al. (1996). The $R-I$ color is significantly bluer than the observations, possibly due to the steeper slope at the red edge of the Si II feature.

#### *3.1.8. 17 March 1994*

The 17 March 1994 observed spectrum of SN 1994D with our best synthetic spectrum at day 16 are shown in Figure 9. The synthetic spectrum fits the observation very well. The shapes of the features match very well. Of note is the fit in the Ca II H+K and blueward, and the fit of the Si II feature at 6150 Å including the slope and 'bend' in the continuum redward of the feature. There is only the small downward continuum shift between these two well fit regions. This shift is reflected in the $V-R$ color which is 0.10 to 0.15 magnitudes redder depending on the comparison observations. The rest of the colors coincide with the observations. For this model the total continuum optical depth at 5000 Å, $\tau_{5000}$, is unity at 9000 km s$^{-1}$. This is the transition point between the partially

burned material and the $^{56}$Ni-rich core.

### *3.1.9. 18 March 1994*

We plot the 18 March 1994 observed spectrum of SN 1994D with our best synthetic spectrum at day 17 in Figure 10. Like day 16, the day 17 spectrum fits the Ca II H+K feature very well. The remaining feature shapes are also good, but the slightly lower continuum level between the Ca II H+K and Si II features remains. Again, this makes the $V-R$ color redder than the observations.

### *3.1.10. 19 March 1994*

Figure 11 displays the 19 March 1994 observed spectrum of SN 1994D with our best synthetic spectrum at day 18. The shape of the fit is good, especially blueward of 4000 Å and redward of 6000 Å. The shape of the features between the Ca II H+K and 6150 Å Si II features is good, but they are shifted to lower flux. This lower flux makes the $V-R$ color redder than the observations.

### *3.1.11. 20 March 1994*

Plotted in Figure 12 is the 20 March 1994 observed spectrum of SN 1994D with our best synthetic spectrum at day 19. The shape of the synthetic spectrum is good. The fit is good blueward of 4000 Å and redward of 6000 Å. The shapes of many of the features between are poor. The overly strong blue Si II feature at 5750 Å indicates that the temperature of the line-forming region is too low. By increasing the luminosity by 40%, the resulting temperature change improves the fit of the blue Si II feature and the S II "W" feature at 5000-5500 Å. This badly changes the shape of the blue part of the synthetic spectrum. These features form in the optically thin zone at this and later epochs. If we could heat this zone without affecting the luminosity the quality of the spectrum could be improved. A viable way to achieve this would be to mix additional $^{56}$Ni into the zone, which is expected in multi-dimensional burning models. The colors are all redder than the observations, particularly $B-V$ and $R-I$, thus suggesting that the luminosity or model temperature is too low.

### 3.2. After Visual Maximum

#### *3.2.1. 23 March 1994*

We plot the 23 March 1994 observed spectrum of SN 1994D with our best synthetic spectrum at day 22 in Figure 13. The shape of this spectrum is good, but the strength of some of the optical features is exaggerated. The S II "W" is far too weak in our synthetic spectrum. The observation shows a sharp edged feature which indicates that the opacity strongly cuts off at higher velocities. This is consistent with the sulfur distribution in W7. In the region of strong sulfur concentration, the sulfur in the W7 model has an ionization ratio $S^{+}/S^{++} \sim 2$. This, along with the temperature sensitive strength of the red Si II feature at 5800 Å, suggests that the ionization temperature should be higher in the zone between the Fe-core and the unburned region in these epochs where they are optically thin. The colors are consistent with the trends in the observations, except the $V-R$, which is affected by the larger fluxes at the S II "W" feature.

#### *3.2.2. 26 March 1994*

We plot the 26 March 1994 observed spectrum of SN 1994D with our best synthetic spectrum at day 25 in Figure 14. As in day 22, the S II "W" is weak and the red Si II feature is too strong. The overall shape of the spectrum appears to be good, but the limited range of the spectral data make a more certain fitting of the blue peaks near Ca II H+K, and therefore the total luminosity, difficult. This is reflected in the colors, which are erratic, and do not follow any general trend. Of particular note is the shift in the synthetic $U-B$ color to redder than the observations, indicating a near-$UV$ deficit in the synthetic spectra.

#### *3.2.3. 28 March 1994*

Plotted in Figure 15 is the 29 March 1994 observed spectrum of SN 1994D with our best synthetic spectrum at day 27. As on day 25 the limited range of the available observed spectrum makes precise fitting of the luminosity difficult. The general difficulties in making the rest of the spectrum fit may be due to problems with the W7 model or with the temperature structure we have calculated in our quasi-static, energy balanced models. The spectrum is also making the nebular transition, the continuum optical depth at 5000 Å, $\tau_{5000} \sim 4$. Like day 25, the colors disagree with the observed photometry.

#### *3.2.4. 31 March 1994*

We plot the 31 March 1994 observed spectrum of SN 1994D with our best synthetic spectrum at day 30 in Figure 16. The minimum wavelength of the 31 March spectrum is only 5500 Å, so we have scaled the 2 April spectrum and added it to Figure 16. We have now switched to nebular boundary conditions because $\tau_{5000} \sim 3$ [see Nugent (1997) and Nugent et al. (1997) for a discussion of our choice of boundary conditions and the results of tests]. This means that we assume that the space inside the innermost zone, at $\sim$ 1000 km s$^{-1}$, is completely transparent. The shape of the spectrum is good and the line features are acceptable. The largest discrepancy is the complete lack of the Na I D feature. This feature has been slowly growing in the observations, but is not replicated in the synthetic spectra. We discuss this in § 5.3. The colors are still erratic, but the $U-B$ is not as excessively red as before.

#### *3.2.5. 2 April 1994*

Figure 17 shows the 2 April 1994 observed spectrum of SN 1994D with our best synthetic spectrum at day 32. This spectrum fits a bit less well than for day 30. Again the strong Na I D feature is missing. Like the day 30 model, the day 32 model uses nebular boundary conditions and the luminosity corresponds to instantaneous re-processing of deposited $\gamma$-ray energy. The continuum optical depth continues to decline and for this model is $\tau_{5000} \sim 2$. The colors continue to be erratic, and the deficit in the near-$UV$ is reflected by the very red $U-B$.

### 3.3. Pre-observation Spectra

We have extended the luminosities found by fitting the earliest spectra using a parabolic luminosity law, $L \propto t^2$, as used by Riess et al. (2000) and Aldering et al. (2000). This form approximates the early SN Ia as a fixed temperature object with a constant *velocity* photosphere. We plot our synthetic spectra using our extended luminosities in Figure 18. To avoid computational problems caused by the sharp density 'spikes' at the edge of the unburned C+O which are close to the photosphere for the day 1 and day 2 models, we have used an exponential density law, $\rho \propto e^{-v/v_e}$, where $v_e = 2700$ km s$^{-1}$ to match the shape of the W7 density profile. The three exponential models (dashed lines) extend to $\sim$ 60000 km s$^{-1}$ and show a much larger $UV$-deficit at the Ca II H+K edge. We have computed another model at day 3 where the outer edge of the ejecta was at $\sim$ 30000 km s$^{-1}$, as it is in W7, demonstrating that the strength of the large $UV$ deficit is related to the extension of the atmosphere. This will be an interesting topic for future modeling of early SNe Ia $UV$ spectra and photometry. The other significant difference between the exponential and regular W7 models is the Ca II IR triplet feature at 8000 Å.

The features in the synthetic spectra evolve during the week after explosion. The Si II feature

becomes weaker for earlier spectra. This behavior is the same as found in Lentz et al. (2000), where some features, including Si II, were formed mostly in the intermediate velocity regions containing freshly formed silicon. At early times, the outer layers are more opaque to the deeper, silicon-rich material and the Si II feature forms in the unenriched C+O layers. Additionally at earlier times, the mass of silicon outside the "photosphere", loosely defined as $\tau_{5000} \sim 1$, is less than later times. This decrease in absorption is also likely the reason for the decreasing strength of the O I feature at 7500 Å. The Fe II feature at 4800 Å is formed in the fast C+O layer as we have discussed in § 3.1.1. The Ca II IR triplet is likely saturated and only changes with the switch to an exponential density profile.

## 4. Synthetic Photometry

We have computed synthetic $UBVRI$ (Bessell 1990) using the prescription of Hamuy et al. (1992), and $JHK$ (M. Hamuy, private communication) photometry from the synthetic spectra presented in § 3. The synthetic photometry are plotted in Figures 19, 20, & 21, and the colors in Figures 22, 23, & 24.

### 4.1. Ultra-Violet Photometry and Colors

We have calculated the photometry for our synthetic spectra in the $UV$ using the Advanced Camera for Surveys (ACS), scheduled to be installed in the Hubble Space Telescope in 2001. We used the ACS Exposure Time Calculator[1] to obtain count rates in each filter and calibrated the results with a Vega calibration spectrum at $V = 15$. The ACS absolute photometry and the count rates for our spectra when observed at $7.5 \times 10^{25}$ cm, $\mu = 31.93$, are reported in Table 3. We can see that with this instrument, accurate $UV$ photometry of SNe Ia which are a few days old are possible with short exposures.

The $UV$ light curves in Figure 19 peak 3–6 days before maximum light in the visual band. This is approximately consistent with the $U$-band peak displacements of -1 day (Richmond et al. 1995) and -2 days (Patat et al. 1996) in the SN 1994D observations and -1 day in the light curve analysis of Vacca & Leibundgut (1996). The peak timing of the $UV$ light curves is also consistent with the report of Kirshner et al. (1993).

The colors (Figure 22) between the three ACS filters are fairly flat with no consistent trend, but with some oscillations as the $UV$ region is the most sensitive to small fitting errors in modeling the synthetic spectra. The F330W-$U$ color is the difference between the 'ACS $U$' and the Bessell (1990) $U$. Though the filters are intended to be equivalent, the large, strong, features of SNe Ia make

[1] `http://garnet.stsci.edu/ACS/ETC/acs_img_etc.html`

simple transformations difficult. These difficulties can be overcome by applying the relevant transformations for the object's reddening and red-shift, and for the observational filter and detector, to the synthetic spectra when generating synthetic photometry for comparison with observations and illustrate the need for synthetic spectra when comparing photometric observations.

### 4.2. Optical Light Curves and Colors

Figure 20 shows that the $U$-band, like the F330W band, peaks about 3–6 days before maximum light consistent with the observations. The $B$, $V$, $R$, and $I$ light curves do not fall as fast after maximum as the observations (Patat et al. 1996; Richmond et al. 1995; Meikle et al. 1996). This is likely due to the large features of the post-maximum spectra that did not fit as well as the pre-maximum spectra.

The colors are plotted in Figure 23. The $U-B$ curve corresponds well with the observations (Patat et al. 1996), getting bluer until $U-B < -0.5$ at about -5 days, then becoming redder until $U-B \sim 0$. The final few models become too $U-B$ red, but this is clearly seen in the $UV$-deficits in the related synthetic spectra. The $B-V$ curves show the same shallow blue minimum near maximum light and slow reddening afterward as in the observations (Richmond et al. 1995; Patat et al. 1996). The $V-R$ curves follow the same blue evolution from $V-R \sim 0.2$ at -10 days to $V-R \sim -0.3$ at +10 days as observed (Richmond et al. 1995; Patat et al. 1996). The $R-I$ color falls from $R-I \sim 0$ at -10 days to $R-I \sim -0.4$ and then returns to $R-I \sim 0$ afterwards as do the observations (Richmond et al. 1995), but the timing of the synthetic colors is ambiguous and possibly earlier than the observations.

### 4.3. IR Photometry and Colors

We have plotted the synthetic infra-red light curves in Figure 21. The $K$-band photometry seems to be consistent with the light curve templates of Elias et al. (1985). The $J$-band is flat rather than falling during the post-maximum period we model, and the $H$-band rises rather than remaining flat. This is likely due to the difficulties noted in § 3.2 with features not fitting well. The pre-maximum $IR$ photometry is flat within fitting scatter for all bands in the 10 days before maximum consistent with the $IR$ photometry of SN 1998bu (Hernandez et al. 2000). The $IR$ colors are presented in Figure 24.

Figure 25 displays the bolometric luminosity which is clearly too flat after maximum (Contrado et al. 2000). We suspect that both the peak is a little too subluminous and that if the postmaximum fits better reproduced the observed colors, we would have better agreement with observed bolometric light curves after maximum. This shows that while the density structure and composition of the outer layers of W7 do a good job of reproducing the observed spectra, the structure of the inner layers is not quite correct.

## 5. Analysis

### 5.1. Identification of the 10500 Å Feature

The identification of the absorption feature at 10500 Å in the spectra of SNe Ia has been the subject of debate. The primary candidates are: He I $\lambda$10830, O I $\lambda$11287, Mg II $\lambda$10926, and Fe II $\lambda$10926. All of these, except He I, are found in W7. We have treated all of these species in NLTE. Meikle et al. (1996) and Mazzali & Lucy (1998) find both Mg II and He I as equally probable. Hatano et al. (1999) found the feature best fit with Mg II. Wheeler et al. (1998) and Marion et al. (2000) have used delayed detonation models of C+O white dwarfs and found that the Mg II provided a good fit and could be used as a diagnostic of the outer edge of the burned material in SN Ia. We have also used a model, W7, that does not contain helium and found that the feature fit well. We have plotted the near-$IR$ spectrum of SN 1994D on 20 March with our best fit model and a diagnostic spectrum in Figure 26. The diagnostic spectrum is generated from the converged atmosphere model and calculated with only Mg II line opacity and no other line opacity. We can see that the 10500 Å feature in all three spectra are of the same strength and at the same wavelength. This feature, which does not shift in wavelength in the observations at earlier epochs (Meikle et al. 1996), is clearly formed by Mg II in our synthetic spectra of W7. This also shows that the abundance of magnesium and the velocity range in W7 corresponds well to that in SN 1994D.

### 5.2. Distance to NGC 4526 and the Luminosity of SN 1994D

We have applied our synthetic photometry of SN 1994D and the many available observed photometric data to derive the distance to NGC 4526 using the Spectral-fitting Expanding Atmospheres Method (SEAM). SEAM determines the distance to a supernova by fitting the spectra of a supernova and deriving a distance modulus, $\mu$, from the synthetic photometry (Baron et al. 1993, 1994, 1995a,b, 1996, 2000). We have used all $U$, $B$, $V$, $R$, $I$ photometry from Richmond et al. (1995), Patat et al. (1996), Meikle et al. (1996), and Tsvetkov & Pavlyuk (1995) that correspond to the dates of the spectra we have fit in § 3. We plot the individual distance moduli obtained from each observation paired with the appropriate synthetic spectrum in Figure 27. The error bars include the stated observational error and our estimate of the fitting error of the model luminosity. For the $U$-band data of Richmond et al. (1995) we have used an error of 0.5 magnitudes to reflect the systematic error suspected by the observers. We have computed an error-weighted mean of the distance modulus and have found the value, $\mu = 30.8 \pm 0.3$, where 0.3 is the 1-$\sigma$ error. The individual band averages range from $\mu = 30.71$ for the $I$-band to $\mu = 30.94$ for the $U$-band. The horizontal line in Figure 27 is a weighted least-squares fit to the distance modulus as a function of epoch. The fit varies by $\sim 0.01$ magnitudes over the range of epochs considered (the slope of the fitted line is 0 to 2 parts in $10^4$). The luminosity of the model atmosphere depends on the radius which is a function of time. Small changes in the timing of the explosion will affect the derived distance. The spectra change slowly enough that a fit can be nearly replicated with a model ex-

panded to an earlier (later) epoch with a lower (higher) luminosity. Each day error in the risetime generates an error of $\sim 0.15$ magnitudes. There are also errors that may arise from deficiencies in the chosen model and the other inputs to the synthetic spectra. We derive the distance modulus to be $\mu = 30.8 \pm 0.10$ (internal) $\pm 0.20$ (timing). This result is consistent within errors with that of Drenkhahn & Richtler (1999) who find $\mu = 30.4 \pm 0.3$ using the globular cluster luminosity function, and with that of Höflich (1995) who used light curve calculations to obtain $\mu = 31.05 \pm 0.05$.

### 5.3. Weak Ca II H+K and Na I D Features

Two concerns about the synthetic spectra are the general weakness of the Ca II H+K feature in the models for the first 12 days after the explosion, and the complete absence of the Na I D feature, which begins to appear about one week after maximum light. To overcome these deficiencies we have attempted many modifications to the models. For the early Ca II H+K problem we have tried extending the models to higher velocities. This does increase the strength of the Ca II IR triplet and Ca II H+K features for the very early exponential models in Figure 18, but does not affect the models which correspond to the observed spectra, because at those later epochs the line forming region has moved into the velocities of our normal W7 model. Increasing the density of the C+O region by decreasing the slope of the density decline did not have a significant effect. We also tried increasing the deposition of $\gamma$-ray energy, but as the problem is over-ionization rather than under ionization, this did not improve the Ca II H+K feature shape. We have also tried extreme abundance enrichment in calcium and sodium to make the corresponding features stronger with inadequate results. Thus, overall it will require modifications to W7 to improve the lineshapes of the Ca II H+K and Na I D features. Since the problem is that e.g., Ca exists primarily as Ca III and we need to increase the Ca II population, this would require higher densities, since lower temperatures would no longer fit the overall shape of the observed spectrum. This could be an indication that non-spherical effects, such as composition asymmetries and clumping are playing a role.

### 5.4. How Good is W7?

The synthetic spectra made with W7 fit the observed spectra of SN 1994D quite well in the pre-maximum epoch, except for the above discussed problem with Ca II H+K. After the continuum 'photosphere', $\tau_{5000} \sim 1$, recedes into the Fe-peak element rich core the quality of the spectral fits begins to break down. The other significant possibility is that the particular density and abundance structure of W7 in the Fe-rich core is not fully reflective of SNe Ia and SN 1994D. Some neutron rich isotopes have been shown to be overproduced in W7 (Iwamoto et al. 1999; Brachwitz et al. 2000).

The other deficiency is in the later pre-maximum spectra where the 4000–6000 Å flux is slightly

low and certain temperature sensitive features, such as Si II, indicate that the line forming region should be hotter. We found that these problems could be at least partially solved by increasing the luminosity, which seems to be required by the synthetic photometry. However, these higher luminosity models fit the blue flux poorly. A model with more $^{56}$Ni mixed into the partially burned silicon and sulfur rich zones would raise the effective temperature of the region that is above $\tau_{5000} = 1$, which could help both the feature shape and the overall agreement with the inferred maximum brightness of SNe Ia. This type of mixing would be expected in the turbulent 3-D models (Khokhlov 2001; Lisewski et al. 2000; Reinecke et al. 1999).

## 6. Conclusions

The SN Ia C+O white dwarf deflagration model works reasonably well in fitting the normal SNe Ia SN 1994D. The fits are particularly good for the week before maximum light. There are some modest problems with the post-maximum spectra that are either due to differences between the W7 Fe-rich core composition and structure and that of SNe Ia, specifically SN 1994D, or due to significant departures from LTE in the temperature, ionization, and level populations of the Fe-peak species in the core which requires a more detailed NLTE treatment. From these results it seems reasonable to infer that the outer parts of W7 reasonably well resemble the outer parts of SNe Ia, whereas the inner parts differ in density, composition, or nickel mixing/clumping. From the synthetic spectra we have computed synthetic photometry. This synthetic photometry combined with the synthetic specrta allow us to use the SEAM method to calculate the distance to NGC 4526, which we find to be $\mu = 30.8 \pm 0.3$. This is a very encouraging demonstration of the potential of the SEAM method applied to SNe Ia.

Observationally, the fitting described in this paper requires spectra that show a rise from the blue, through the peak of the distribution, to the red tail. Practically, this means spectra covering the range 3100–8000 Å, preferably extending to 10000 Å or beyond. Near-$UV$ spectra and photometry are also needed for at least some objects, so that we might understand what variability exists in the near-$UV$. We hope that to have demonstrated that this data is accessible with the current generation of instruments for SNe Ia out to $\mu \sim 32$. Early discovery and monitoring are also important since we can probe the outermost layers of SNe Ia only at these early times and hopefully better constrain the risetimes of SNe Ia as a group and individually.

We plan to consider additional explosion models, peculiar SNe Ia, and infra-red spectra in more detail. Part of our efforts will be to test the effects of more complete NLTE treatment of all relevant ionic species in the opacity. We are also working to include non-equilibrium temperature evolution effects through the calculation of light curves.

We thank Mario Hamuy for providing us with the infrared filter and atmospheric transmission functions and for helpful discussions on their proper interpretation and use. We also thank Alex

Filippenko, Ferdinando Patat, Nic Walton, Jim Lewis, and Peter Meikle for providing us with their observed spectra and photometry. This work was supported in part by NSF grant AST-9731450, NASA grant NAG5-3505, and an IBM SUR grant to the University of Oklahoma; and by NSF grant AST-9720704, NASA ATP grant NAG 5-8425, and LTSA grant NAG 5-3619 to the University of Georgia. PHH was supported in part by the Pôle Scientifique de Modélisation Numérique at ENS-Lyon. Some of the calculations presented in this paper were performed at the San Diego Supercomputer Center (SDSC), supported by the NSF, and at the National Energy Research Supercomputer Center (NERSC), supported by the U.S. DOE. We thank both these institutions for a generous allocation of computer time.

## REFERENCES

Aldering, G., Knop, R., & Nugent, P. 2000, AJ, 119, 2110

Baron, E., Hauschildt, P. H., & Branch, D. 1994, ApJ, 426, 334

Baron, E., Hauschildt, P. H., Branch, D., Austin, S., Garnavich, P., Ann, H. B., Wagner, R. M., Filippenko, A. V., Matheson, T., & Liebert, J. 1995a, ApJ, 441, 170

Baron, E., Hauschildt, P. H., Branch, D., Kirshner, R. P., & Filippenko, A. V. 1996, MNRAS, 279, 779

Baron, E., Hauschildt, P. H., Branch, D., Wagner, R. M., Austin, S. J., Filippenko, A. V., & Matheson, T. 1993, ApJ, 416, L21

Baron, E., Hauschildt, P. H., & Young, T. R. 1995b, Physics Reports, 256, 23

Baron, E. et al. 2000, ApJ, 545, 444

Bessell, M. S. 1990, PASP, 102, 1181

Brachwitz, F., Dean, D., Hix, W. R., Iwamoto, K., Langanke, K., Martinez-Pinedo, G., Nomoto, K., Strayer, M., Thielemann, F.-K., & Umeda, H. 2000, ApJ, 536, 934

Branch, D., Livio, M., Yungelson, L., Boffi, F., & Baron, E. 1995, PASP, 107, 1019

Cardelli, J. A., Clayton, G. C., & Mathis, J. S. 1989, ApJ, 345, 245

Colgate, S., Petschek, A., & Kriese, J. T. 1980, ApJ, 237, L81

Contrado, G., Leibundgut, B., & Vacca, W. 2000, A&A, 359, 876

Cumming, R., Lundqvist, P., Smith, L., Pettini, M., & King, D. 1996, MNRAS, 283, 1355

Drenkhahn, G. & Richtler, T. 1999, A&A, 349, 877

Elias, J. H., Frogel, J. A., Hackwell, J. A., & Persson, S. E. 1985, ApJ, 296, 379

Filippenko, A. V. 1997, in Thermonuclear Supernovae, ed. P. Ruiz-Lapuente, R. Canal, & J. Isern (Dordrecht: Kluwer), 1

Hamuy, M., Walker, A. R., Suntzeff, N. B., Gigoux, P., Heathcote, S. R., & Phillips, M. M. 1992, PASP, 104, 533

Hatano, K., Branch, D., Baron, E., & Fisher, A. 1999, ApJ, 525, 881

Hauschildt, P. H. & Baron, E. 1999, J. Comp. Applied Math., 109, 41

Hernandez, M. et al. 2000, MNRAS, 319, 223

Höflich, P. 1995, ApJ, 443, 89

Höflich, P., Khokhlov, A., Wheeler, J. C., Nomoto, K., & Thielemann, F.-K. 1997, in Thermonuclear Supernovae, ed. P. Ruiz-Lapuente, R. Canal, & J. Isern (Dordrecht: Kluwer), 659

Iwamoto, K., Brachwitz, F., Nomoto, K., Kishimoto, N., Hix, W. R., & Thielemann, F.-K. 1999, ApJ Suppl., 125, 439

Jha, S. et al. 1999, ApJ Suppl., 125, 73

Khokhlov, A. 2001, ApJ, submitted, astro-ph/0008463

Kirshner, R. P. et al. 1993, ApJ, 415, 589

Lentz, E., Baron, E., Branch, D., Hauschildt, P. H., & Nugent, P. 2000, ApJ, 530, 966

Lisewski, A. M., Hillebrandt, W., Woosley, S. E., Niemeyer, J. C., & Kerstein, A. R. 2000, ApJ, 537, 405

Livio, M. 1999, in Type Ia Supernovae: Theory and Cosmology (Cambridge: Cambridge Univ. Press), astro–ph/9903264

Marion, G. H., Höflich, P., & Wheeler, J. C. 2000, RevMexAA, astro-ph/0006414

Mazzali, P. A. & Lucy, L. B. 1998, MNRAS, 295, 428

Meikle, W. P. S. et al. 1996, MNRAS, 281, 263

Nugent, P., Baron, E., Branch, D., Fisher, A., & Hauschildt, P. 1997, ApJ, 485, 812

Nugent, P., Baron, E., Hauschildt, P., & Branch, D. 1995, ApJ, 441, L33

Nugent, P. E. 1997, PhD thesis, University of Oklahoma

Patat, F. et al. 1996, MNRAS, 278, 111

Perlmutter, S. et al. 1999, ApJ, 517, 565

Reinecke, M., Hillebrandt, W., & Niemeyer, J. C. 1999, A&A, 347, 739

Richmond, M. W. et al. 1995, AJ, 109, 2121

Riess, A., Filippenko, A. V., Li, W., & Schmidt, B. P. 2000, AJ, 118, 2668

Riess, A. et al. 1998, AJ, 116, 1009

Salvo, M. E., Cappellaro, E., Mazzali, P., Benetti, S., Danziger, I. J., Patat, F., & Turatto, M. 2001, MNRAS, 321, 254

Sutherland, P. & Wheeler, J. C. 1984, ApJ, 280, 282

Treffers, R. R., Filippenko, A. V., & Van Dyk, S. D. 1994, IAU Circ., 5946

Tsvetkov, D. Y. & Pavlyuk, N. N. 1995, Astronomy Letters, 21, 606

Vacca, W. D. & Leibundgut, B. 1996, ApJ, 471, L37

Wang, L., Wheeler, J. C., & Höflich, P. 1997, ApJ, 476, L27

Wells, L. A. et al. 1994, AJ, 108, 2233

Wheeler, J. C., Höflich, P., Harkness, R. P., & Spyromilio, J. 1998, ApJ, 496, 908

AAS LaTeX macros v5.0.

Table 1. Synthetic Photometry of Best-Fit Models

| Epoch[a] | U | B | V | R | I | J | H | K |
|---|---|---|---|---|---|---|---|---|
| 1[b] | -11.57 | -12.13 | -13.03 | -13.30 | -13.19 | -13.76 | -13.80 | -13.80 |
| 2[b] | -13.42 | -13.82 | -14.55 | -14.66 | -14.60 | -15.08 | -15.07 | -14.94 |
| 3[b] | -14.69 | -14.97 | -15.45 | -15.46 | -15.45 | -15.77 | -15.73 | -15.51 |
| 3[c] | -14.82 | -14.90 | -15.45 | -15.45 | -15.43 | -15.74 | -15.75 | -15.50 |
| 3 | -15.01 | -14.95 | -15.41 | -15.44 | -15.52 | -15.73 | -15.73 | -15.59 |
| 4 | -15.89 | -15.63 | -16.02 | -16.02 | -16.11 | -16.24 | -16.23 | -16.06 |
| 5 | -16.48 | -16.16 | -16.45 | -16.47 | -16.56 | -16.63 | -16.60 | -16.41 |
| 6 | -16.97 | -16.55 | -16.79 | -16.83 | -16.90 | -16.95 | -16.90 | -16.67 |
| 7 | -17.38 | -16.88 | -17.09 | -17.15 | -17.19 | -17.21 | -17.13 | -16.86 |
| 8 | -17.58 | -17.09 | -17.29 | -17.38 | -17.42 | -17.41 | -17.31 | -16.96 |
| 9 | -18.39 | -17.68 | -17.69 | -17.79 | -17.78 | -17.67 | -17.45 | -16.90 |
| 10 | -18.87 | -18.04 | -17.98 | -18.17 | -18.19 | -18.14 | -18.03 | -17.82 |
| 11 | -18.84 | -18.12 | -18.03 | -18.14 | -18.06 | -17.85 | -17.63 | -16.98 |
| 12 | -19.26 | -18.49 | -18.39 | -18.55 | -18.47 | -18.25 | -18.10 | -17.79 |
| 14 | -19.71 | -18.84 | -18.69 | -18.76 | -18.43 | -18.15 | -17.93 | -17.54 |
| 15 | -19.43 | -18.76 | -18.71 | -18.76 | -18.44 | -18.02 | -17.78 | -17.30 |
| 16 | -19.88 | -19.10 | -18.95 | -19.12 | -18.88 | -18.42 | -18.23 | -17.94 |
| 17 | -19.43 | -18.76 | -18.71 | -18.76 | -18.44 | -18.02 | -17.78 | -17.30 |
| 18 | -19.68 | -19.11 | -18.99 | -19.15 | -18.94 | -18.55 | -18.41 | -18.12 |
| 19 | -19.43 | -19.02 | -19.09 | -19.10 | -18.93 | -18.69 | -18.64 | -18.44 |
| 22 | -19.36 | -19.06 | -19.11 | -18.73 | -18.33 | -18.19 | -18.11 | -17.39 |
| 25 | -18.55 | -18.74 | -19.11 | -18.75 | -18.57 | -18.42 | -18.60 | -17.67 |
| 27 | -18.19 | -18.66 | -19.13 | -18.76 | -18.62 | -18.44 | -18.78 | -17.72 |
| 30 | -18.57 | -18.75 | -19.18 | -18.74 | -18.64 | -18.23 | -18.82 | -17.15 |
| 32 | -17.57 | -18.27 | -19.02 | -18.59 | -18.68 | -18.36 | -19.16 | -17.24 |

[a]Days after explosion.

[b]Exponential density profile of C+O composition

[c]Exponential density profile with C+O composition.
Maximum velocity, $\sim 30000$ km s$^{-1}$.

[d]As can be seen the value of $M_{B_{\max}}$, the peak luminosity is a bit low ($\sim$ 0.3 mag), which reflects some shortcomings of the intermediate velocity parts of the W7 model.

Table 2. Color Comparison

| | U-B | | B-V | | V-R | | R-I | |
|---|---|---|---|---|---|---|---|---|
| Epoch[a] | syn | obs | syn | obs | syn | obs | syn | obs |
| 8[b] | -.45 | ··· | .27 | .21 | .13 | .07 | .09 | ··· |
| 9[d] | -.67 | -.22 | .07 | -.07 | .15 | .17 | .04 | -.08 |
| 9[e] | | ··· | | ··· | | .15 | | .12 |
| 10[b] | -.78 | ··· | .01 | -.05 | .23 | .12 | .07 | -.04 |
| 10[c] | | -.37 | | -.01 | | .16 | | -.13 |
| 10[d] | | -.43 | | -.04 | | .13 | | -.02 |
| 10[e] | | ··· | | ··· | | .16 | | .09 |
| 11[b] | -.67 | -.97 | -.04 | .00 | .16 | .14 | -.03 | -.06 |
| 11[c] | | -.47 | | -.02 | | .23 | | -.14 |
| 11[d] | | -.47 | | .00 | | .18 | | .06 |
| 11[e] | | ··· | | ··· | | .30 | | .23 |
| 12[b] | -.73 | -.85 | -.04 | -.01 | .21 | .12 | -.04 | -.08 |
| 12[c] | | -.56 | | .00 | | .24 | | -.17 |
| 14[b] | -.83 | -.62 | -.09 | -.01 | .11 | .08 | -.27 | -.07 |
| 14[c] | | -.62 | | -.03 | | .14 | | -.12 |
| 14[d] | | -.58 | | -.10 | | .10 | | -.05 |
| 14[e] | | ··· | | ··· | | .15 | | -.03 |
| 15[b] | -.63 | ··· | .02 | -.06 | .09 | .03 | -.27 | -.02 |
| 15[c] | | -.60 | | -.07 | | .13 | | -.14 |
| 15[d] | | -.59 | | -.14 | | .17 | | -.07 |
| 16[b] | -.74 | ··· | -.08 | .00 | .21 | .03 | -.18 | -.09 |
| 16[c] | | -.58 | | -.09 | | .10 | | -.17 |
| 16[d] | | -.58 | | -.12 | | .17 | | -.15 |
| 17[b] | -.76 | -.95 | -.09 | .00 | .19 | -.03 | -.21 | -.16 |
| 17[c] | | -.58 | | -.09 | | .06 | | -.26 |
| 18[b] | -.53 | -.95 | -.06 | .00 | .21 | -.03 | -.16 | -.18 |
| 18[c] | | -.56 | | -.07 | | .03 | | -.31 |
| 19[b] | -.36 | -.89 | .12 | -.03 | .06 | -.03 | -.12 | -.27 |
| 19[c] | | -.51 | | -.08 | | .01 | | -.31 |
| 19[e] | | ··· | | -.11 | | .05 | | -.23 |
| 22 | -.25 | | .11 | | -.34 | | -.34 | |

Table 2—Continued

| | U-B | | B-V | | V-R | | R-I | |
|---|---|---|---|---|---|---|---|---|
| Epoch[a] | syn | obs | syn | obs | syn | obs | syn | obs |
| 25[b] | .24 | -.30 | .42 | .11 | -.31 | -.09 | -.13 | -.35 |
| 25[c] | | ··· | | .05 | | .01 | | ··· |
| | | ··· | | ··· | | -.06 | | -.38 |
| 27[b] | .51 | -.42 | .53 | .16 | -.32 | -.15 | -.09 | -.35 |
| 27[c] | | ··· | | .15 | | -.05 | | ··· |
| | | ··· | | ··· | | -.06 | | -.35 |
| 30[b] | .22 | -.26 | .49 | .23 | -.39 | -.18 | -.05 | -.22 |
| 30[c] | | ··· | | ··· | | ··· | | -.37 |
| 32[b] | .74 | -.31 | .81 | .39 | -.38 | -.16 | .14 | -.12 |
| 32[c] | | -.05 | | .27 | | ··· | | ··· |

[a]Days after explosion.

[b]Data from Richmond et al. (1995).

[c]Data from Patat et al. (1996).

[d]Data from Meikle et al. (1996) using Jacobus Kapteyn Telescope.

[e]Data from Meikle et al. (1996) using Issac Newton Telescope.

Table 3. HST ACS Synthetic Photometry

| | Magnitude | | | Count Rate | | |
|---|---|---|---|---|---|---|
| Epoch[a] | F330W | F250W | F220W | F330W | F250W | F220W |
| 1[b] | -10.47 | -8.86 | -6.73 | 5.73 | .87 | .07 |
| 2[b] | -12.46 | -11.18 | -8.96 | 35.56 | 7.35 | .58 |
| 3[b] | -14.24 | -12.89 | -11.16 | 183.97 | 35.47 | 4.42 |
| 3[c] | -14.63 | -13.28 | -11.50 | 262.76 | 50.72 | 6.02 |
| 3 | -13.61 | -12.26 | -10.02 | 102.93 | 19.81 | 1.55 |
| 4 | -15.75 | -14.30 | -12.47 | 740.02 | 129.45 | 14.77 |
| 5 | -16.36 | -14.92 | -12.81 | 1298.30 | 230.24 | 20.20 |
| 6 | -16.93 | -15.54 | -13.37 | 2195.12 | 407.04 | 33.79 |
| 7 | -17.41 | -16.16 | -14.07 | 3422.05 | 722.22 | 64.44 |
| 8 | -17.54 | -16.03 | -14.01 | 3839.12 | 638.16 | 60.60 |
| 9 | -18.52 | -17.11 | -14.83 | 9466.57 | 1724.80 | 128.85 |
| 10 | -19.22 | -18.35 | -16.65 | 18108.65 | 5403.09 | 690.96 |
| 11 | -19.07 | -18.00 | -16.12 | 15671.64 | 3900.93 | 423.30 |
| 12 | -19.57 | -18.58 | -16.75 | 25029.80 | 6712.84 | 757.36 |
| 14 | -20.11 | -19.14 | -17.31 | 40829.55 | 11160.32 | 1271.70 |
| 15 | -19.57 | -18.26 | -16.54 | 24985.13 | 4960.63 | 625.50 |
| 16 | -20.22 | -19.17 | -17.30 | 45226.13 | 11464.97 | 1257.49 |
| 17 | -20.34 | -19.22 | -17.18 | 50561.80 | 12045.89 | 1129.03 |
| 18 | -19.86 | -18.80 | -16.93 | 32516.13 | 8165.91 | 897.51 |
| 19 | -19.38 | -17.65 | -15.48 | 20898.99 | 2826.09 | 236.23 |
| 22 | -19.00 | -17.05 | -14.85 | 14799.15 | 1634.24 | 131.61 |
| 25 | -17.68 | -16.03 | -13.76 | 4364.39 | 635.58 | 48.50 |
| 27 | -17.00 | -15.65 | -13.42 | 2328.59 | 450.16 | 35.16 |
| 30 | -17.92 | -16.25 | -13.96 | 5445.12 | 783.58 | 58.06 |
| 32 | -16.37 | -15.22 | -12.94 | 1310.45 | 302.33 | 22.61 |

[a]Days after explosion.

[b]Exponential density profile of C+O composition

[c]Exponential density profile with C+O composition. Maximum velocity, $\sim 30000$ km s$^{-1}$.

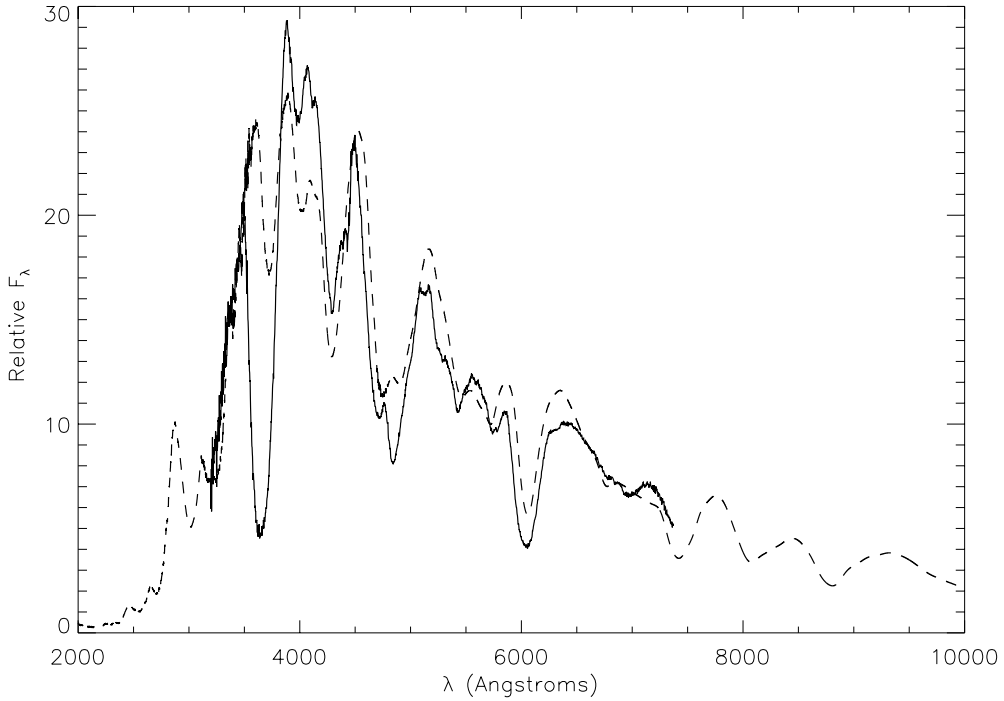


Fig. 1.— SN 1994D on 9 March 1994 (**?**, solid line,)]filipasi97 and W7 best fit synthetic spectrum for day 8 after explosion (dashed line).

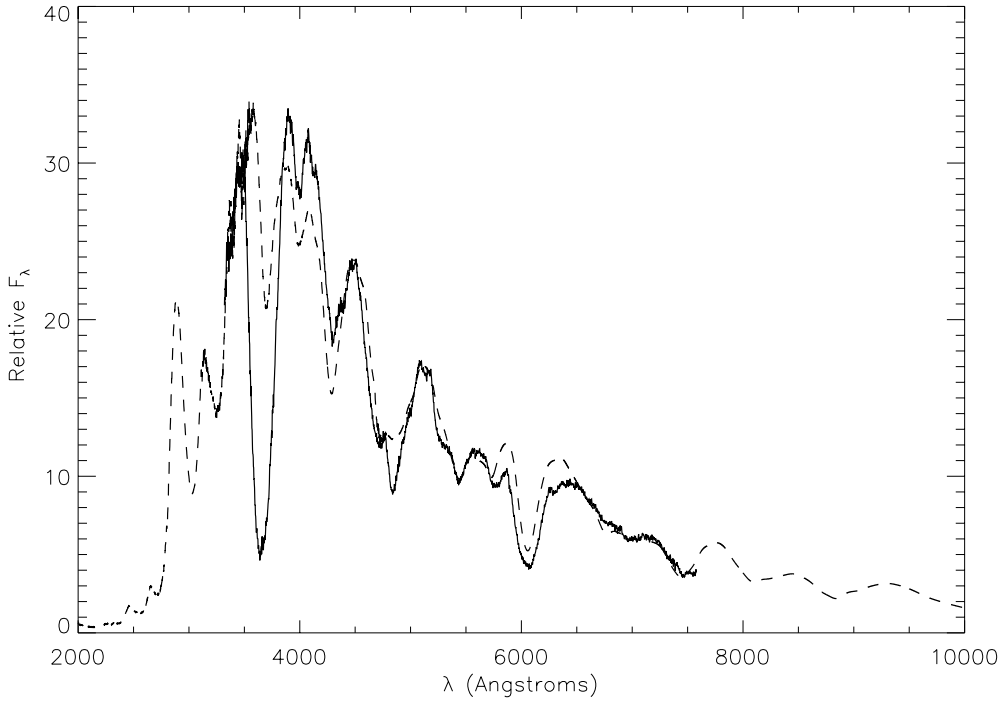


Fig. 2.— SN 1994D on 10 March 1994 (**?**, solid line,)]filipasi97 and W7 best fit synthetic spectrum for day 9 after explosion (dashed line).

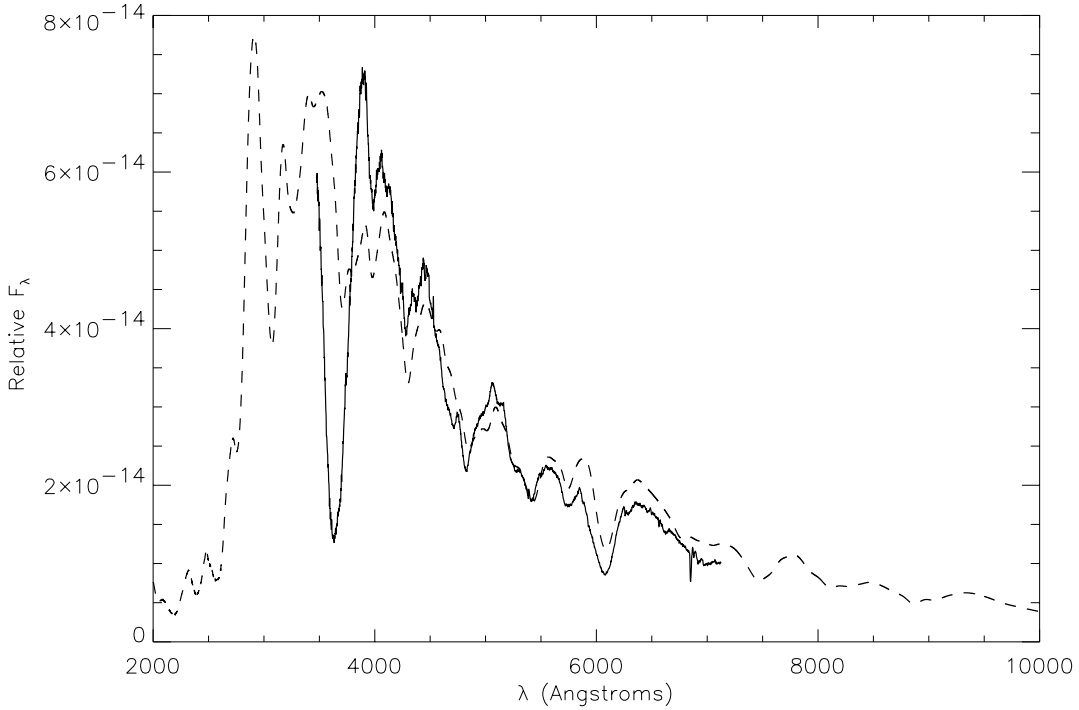


Fig. 3.— SN 1994D on 11 March 1994 (**?**, solid line,)]patat94D96 and W7 best fit synthetic spectrum for day 10 after explosion (dashed line).

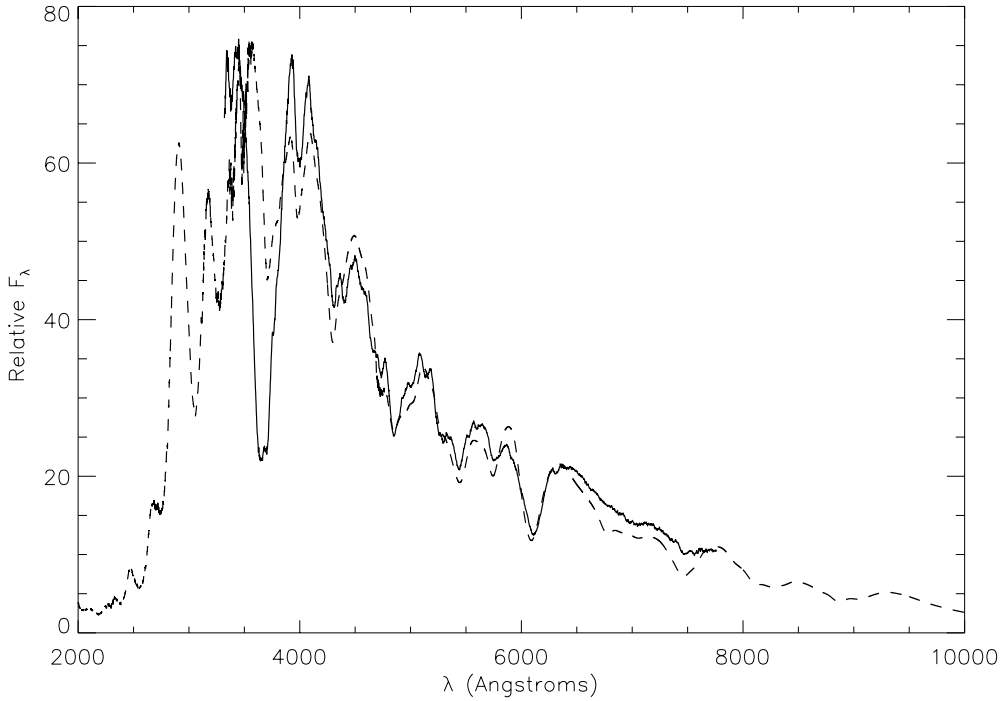


Fig. 4.— SN 1994D on 12 March 1994 (**?**, solid line,)]filipasi97 and W7 best fit synthetic spectrum for day 11 after explosion (dashed line).

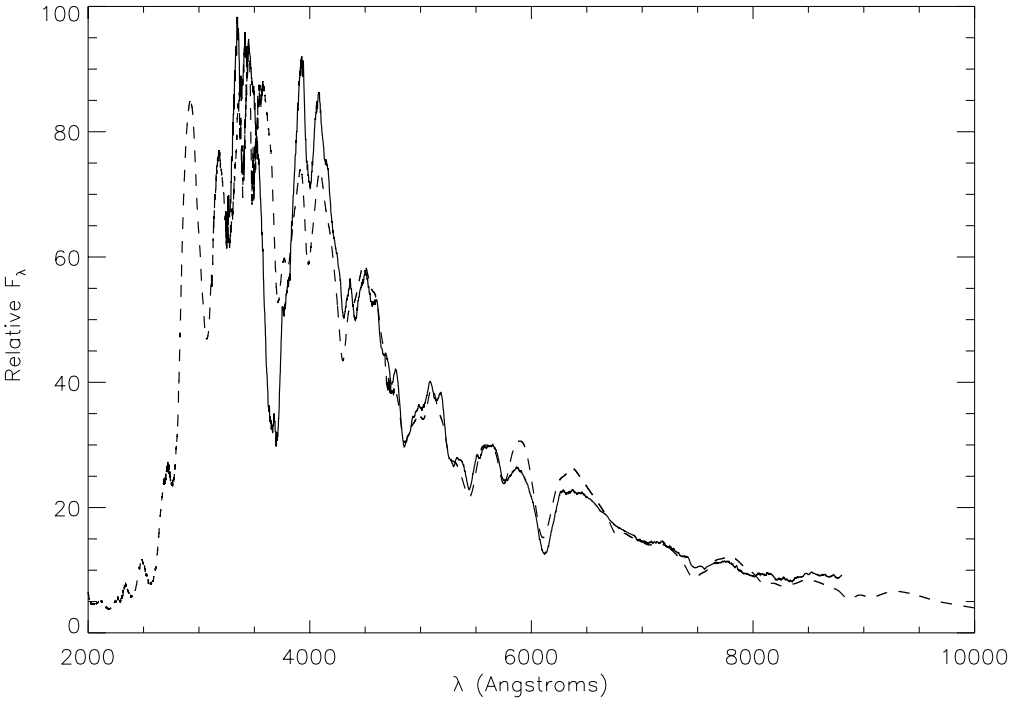


Fig. 5.— SN 1994D on 13 March 1994 (**?**, solid line,)]filipasi97 and W7 best fit synthetic spectrum for day 12 after explosion (dashed line).

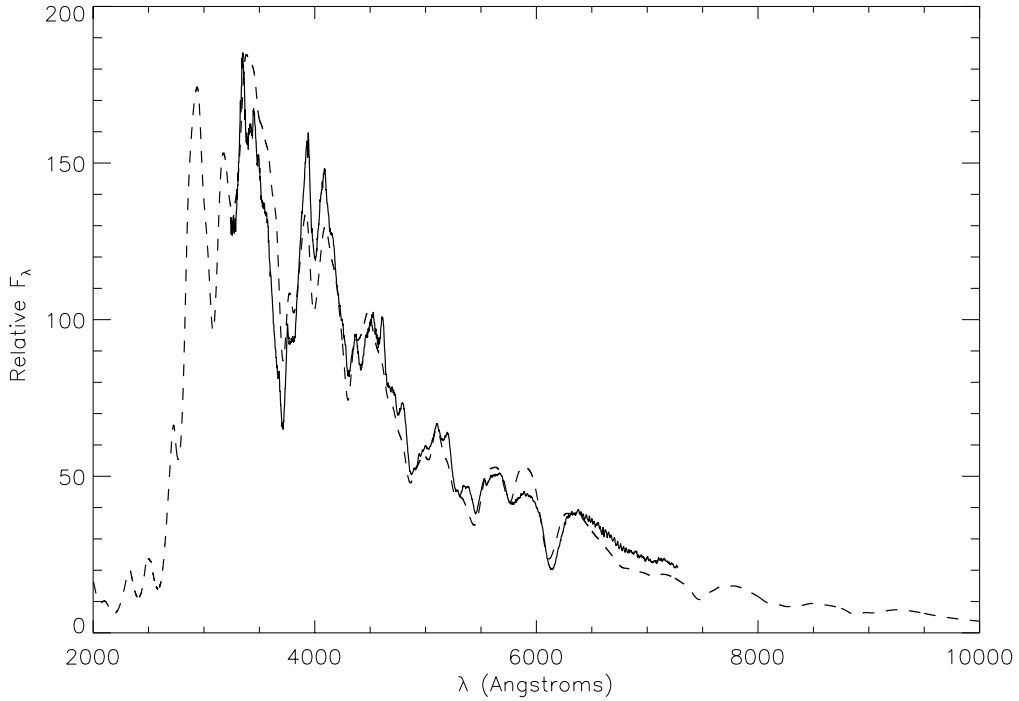


Fig. 6.— SN 1994D on 15 March 1994 (**?**, solid line,)]filipasi97 and W7 best fit synthetic spectrum for day 14 after explosion (dashed line).

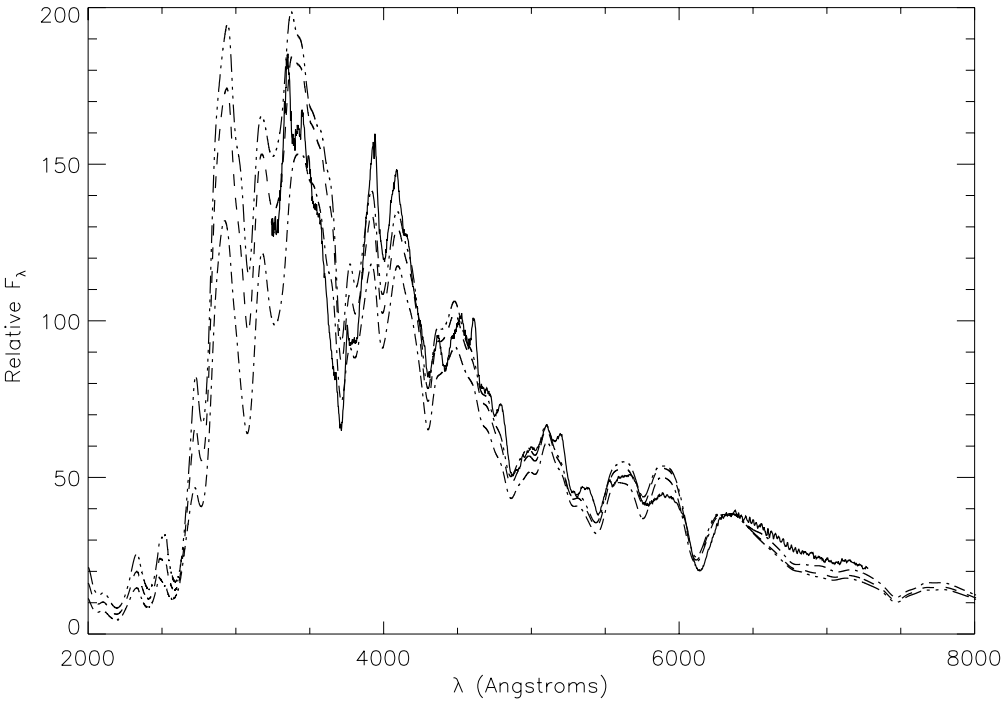


Fig. 7.— SN 1994D on 15 March 1994 (**?**, solid line,)]filipasi97, W7 best fit (dashed line), best fit -7% luminosity (dot-dashed line), and best fit +7% luminosity (dot-dot-dashed line) synthetic spectra for day 14 after explosion.

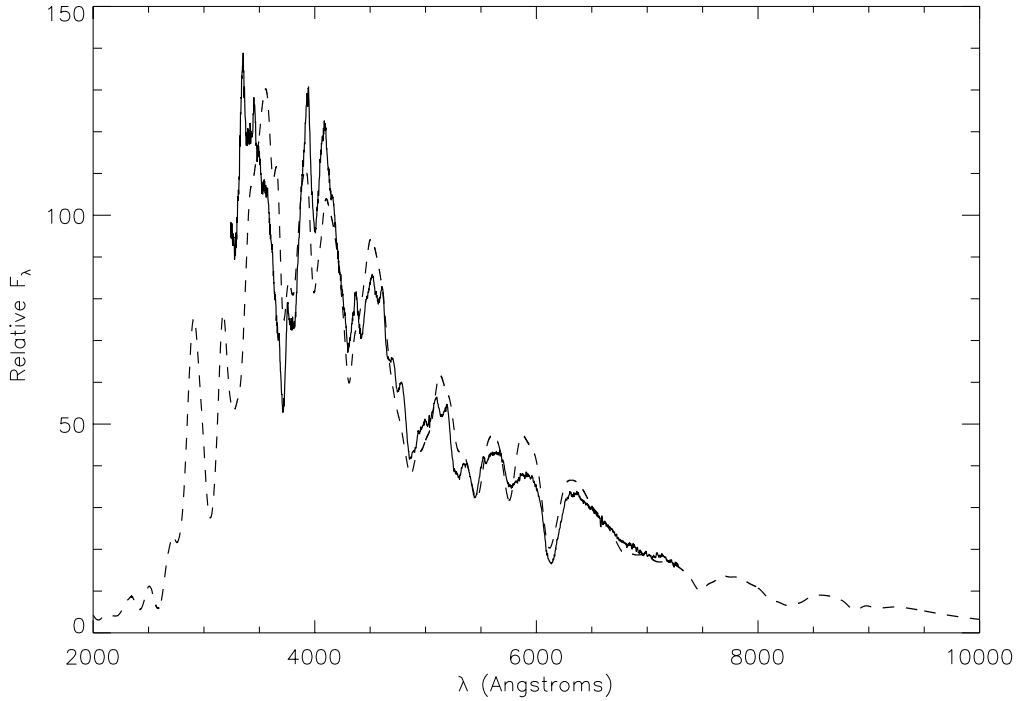


Fig. 8.— SN 1994D on 16 March 1994 (solid line, Filippenko 1994, private communication) and W7 best fit synthetic spectrum for day 15 after explosion (dashed line).

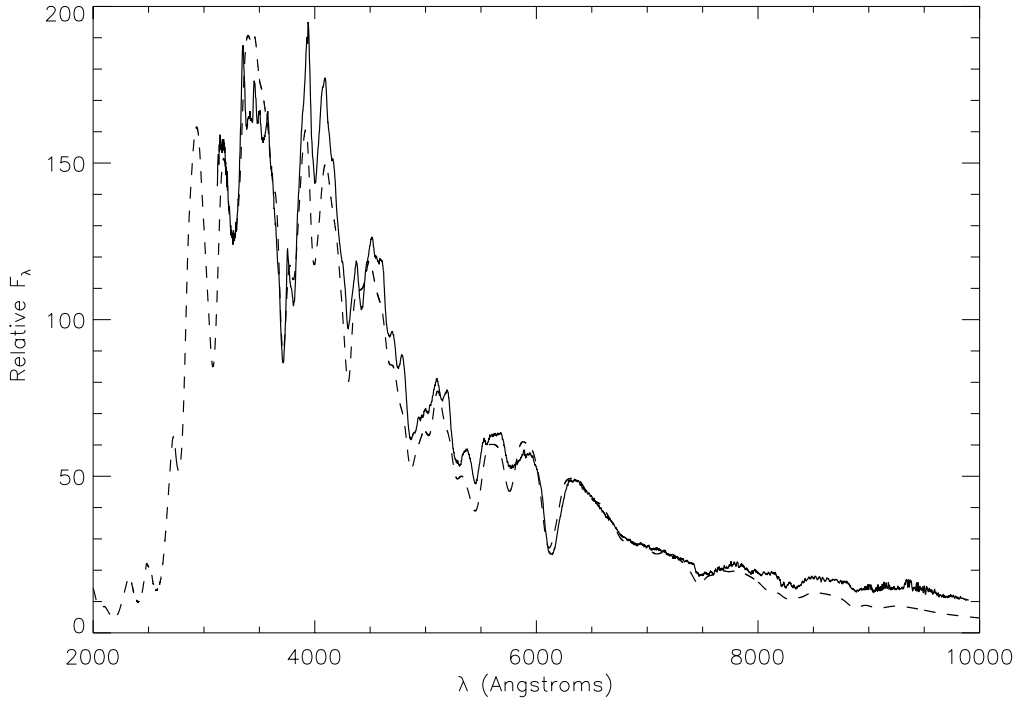


Fig. 9.— SN 1994D on 17 March 1994 (solid line, Filippenko 1994, private communication) and W7 best fit synthetic spectrum for day 16 after explosion (dashed line).

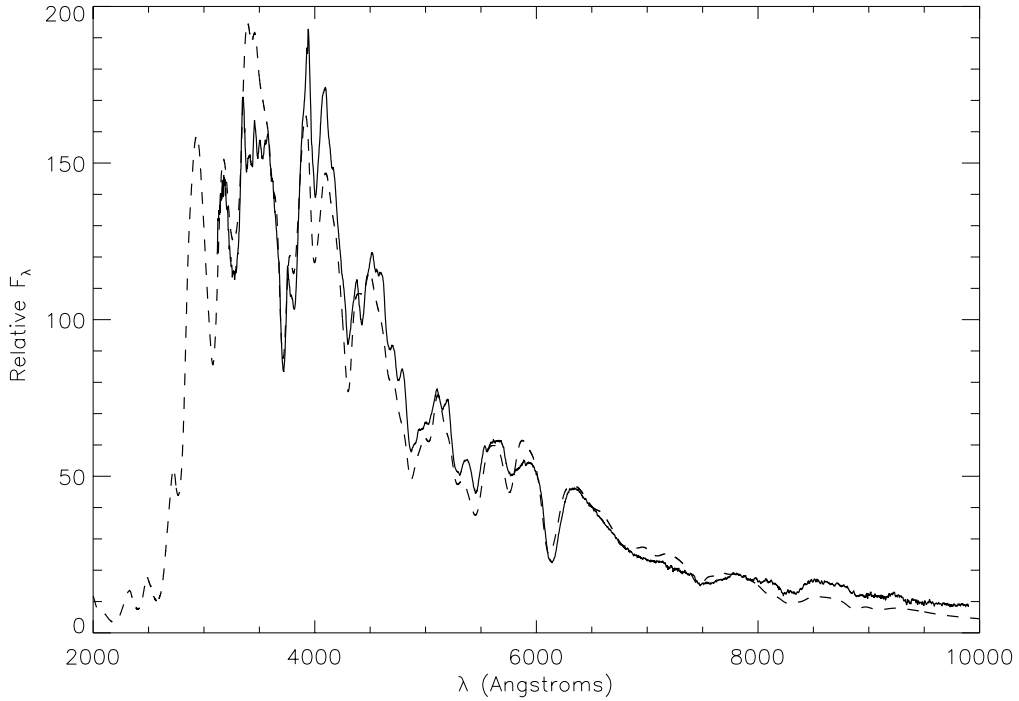


Fig. 10.— SN 1994D on 18 March 1994 (**?**, solid line,)]filipasi97 and W7 best fit synthetic spectrum for day 17 after explosion (dashed line).

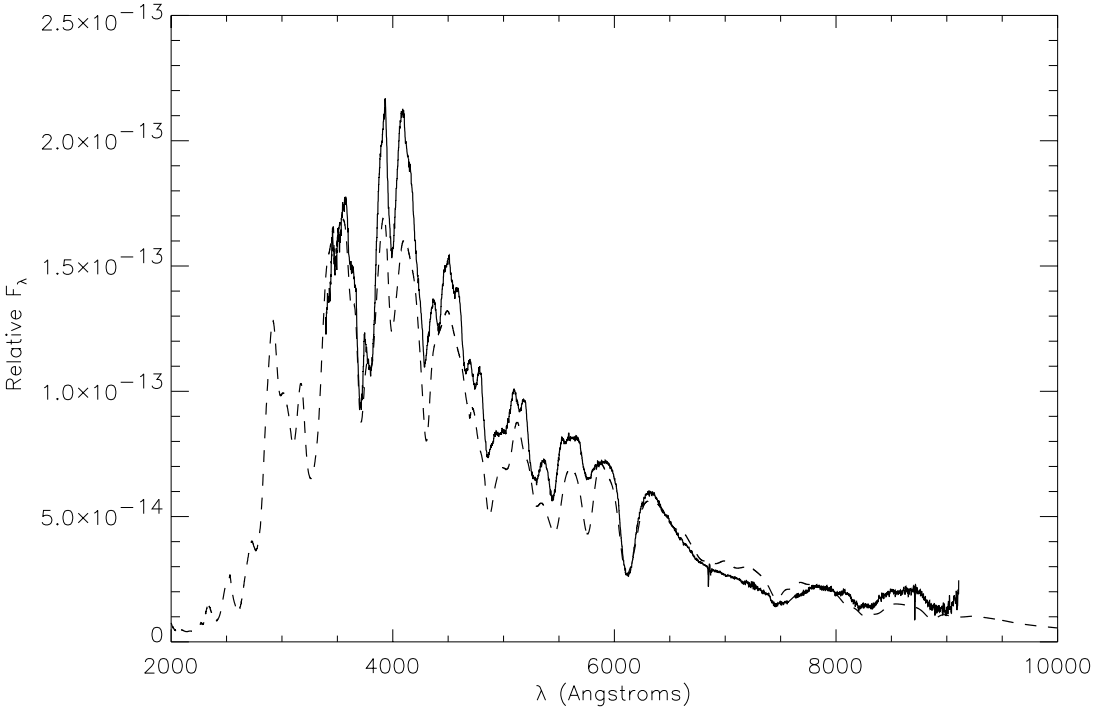


Fig. 11.— SN 1994D on 19 March 1994 (**?**, solid line,)]patat94D96 and W7 best fit synthetic spectrum for day 18 after explosion (dashed line).

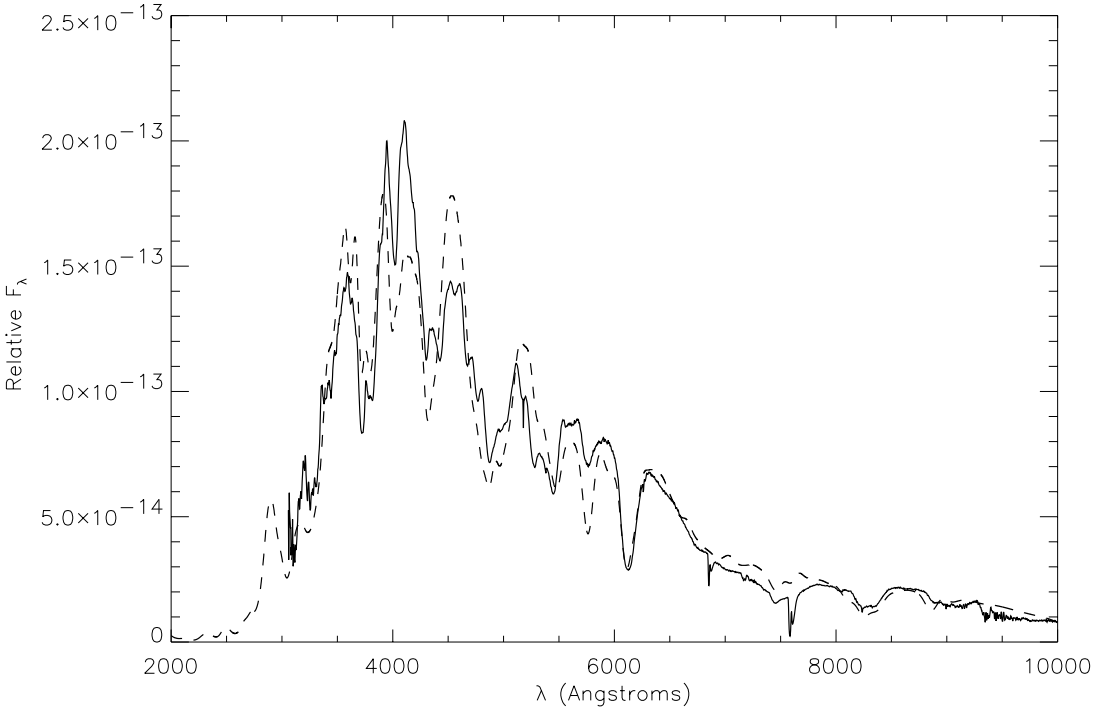


Fig. 12.— SN 1994D on 20 March 1994 (solid line, data obtained on the WHT with ISIS by Nic Walton and reduced at the RGO by Jim Lewis, private communication) and W7 best fit synthetic spectrum for day 19 after explosion (dashed line).

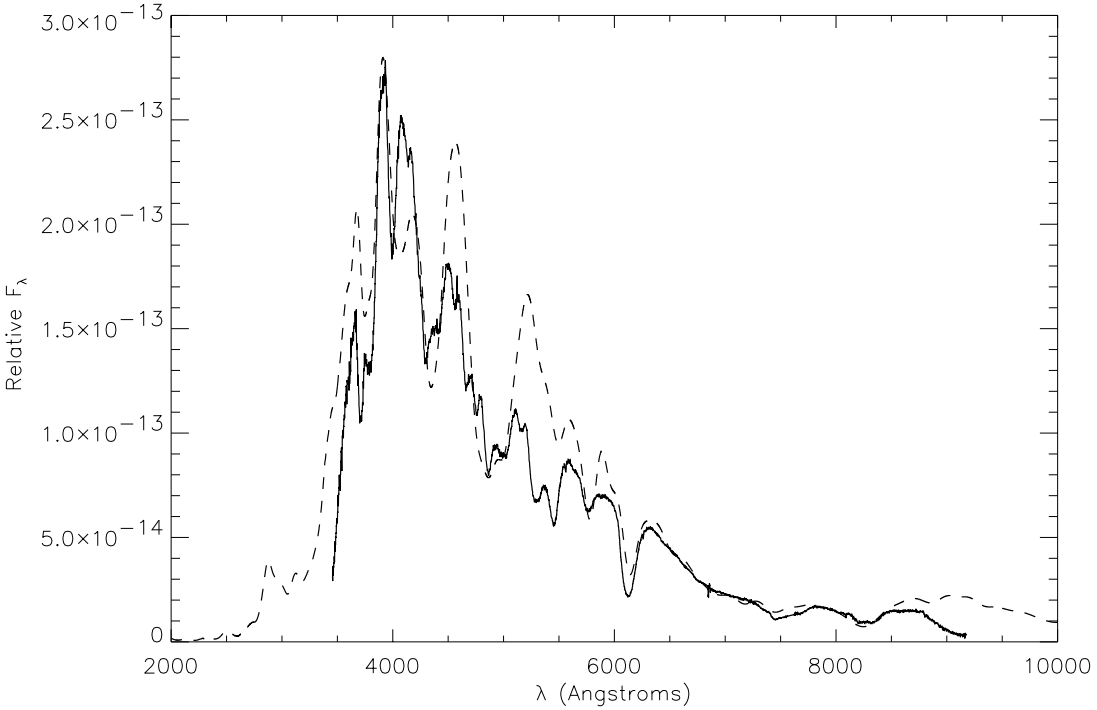


Fig. 13.— SN 1994D on 23 March 1994 (**?**, solid line,)]patat94D96 and W7 best fit synthetic spectrum for day 22 after explosion (dashed line).

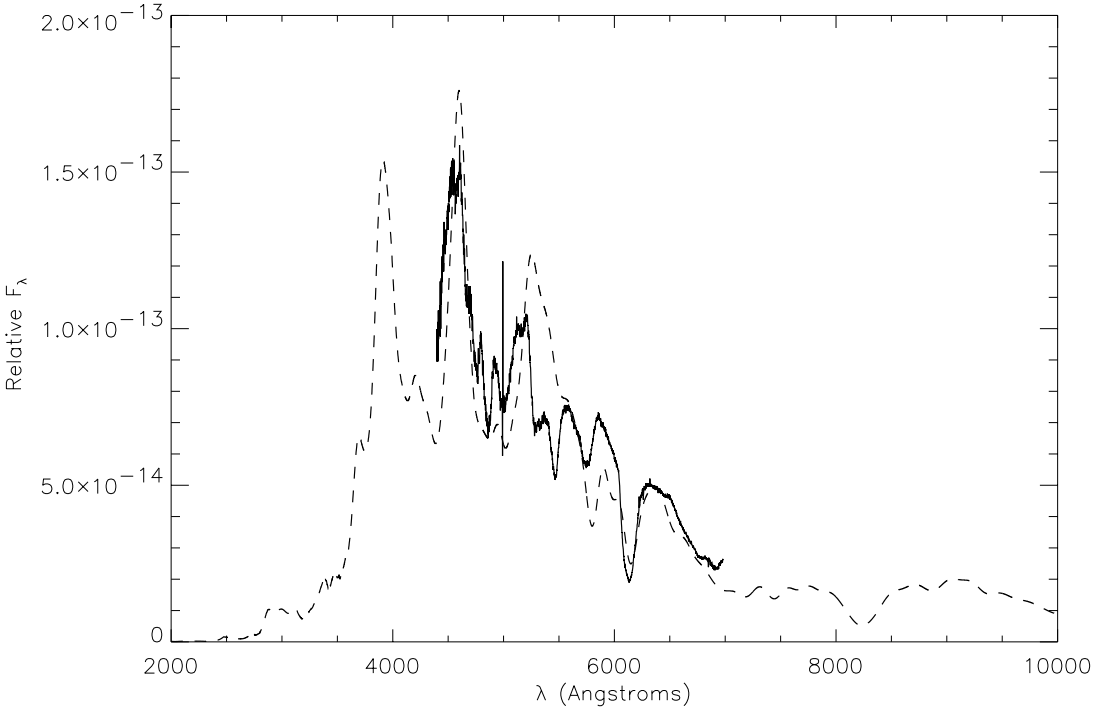


Fig. 14.— SN 1994D on 26 March 1994 (**?**, solid line,)]patat94D96 and W7 best fit synthetic spectrum for day 25 after explosion (dashed line).

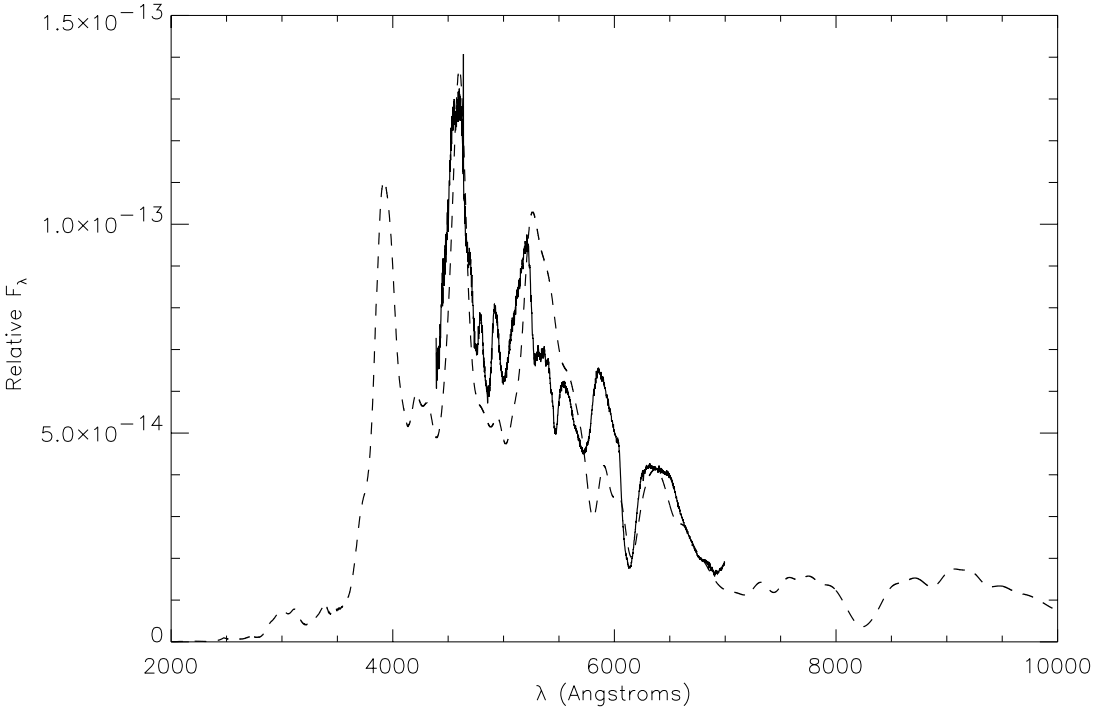


Fig. 15.— SN 1994D on 28 March 1994 (**?**, solid line,)]patat94D96 and W7 best fit synthetic spectrum for day 27 after explosion (dashed line).

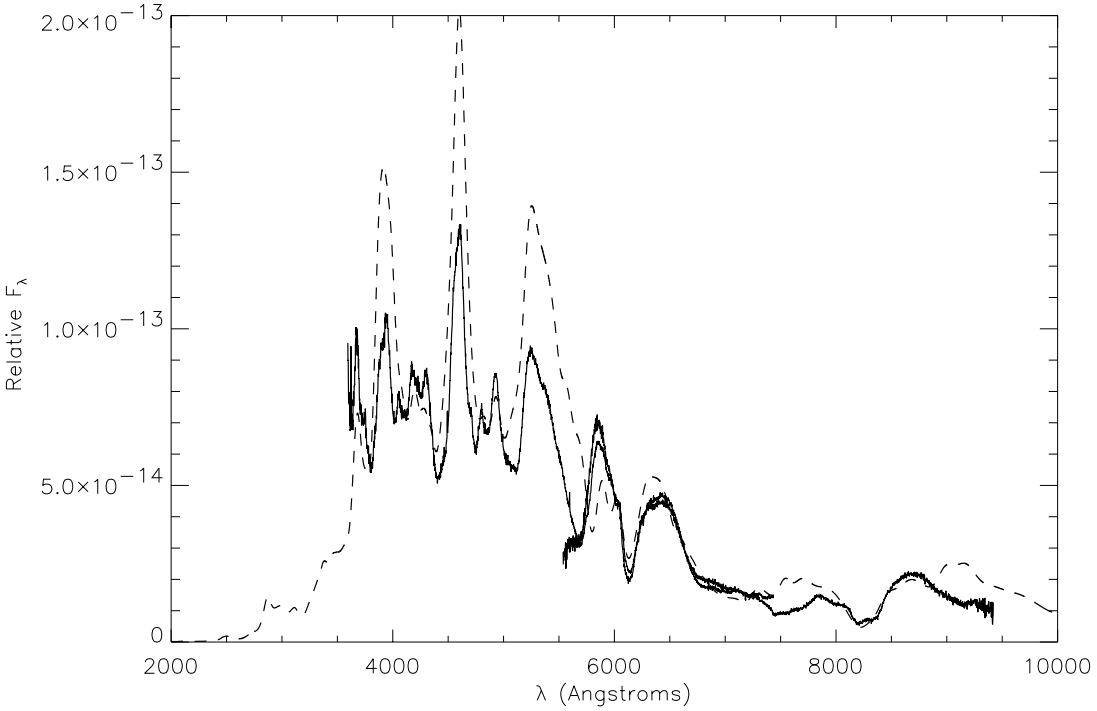


Fig. 16.— SN 1994D on 31 March 1994 (**?**, solid line, red portion,)]patat94D96 and W7 best fit synthetic spectrum for day 30 after explosion (dashed line). The scaled spectrum from 2 April 1994 (**?**, solid line, blue portion,)]patat94D96 has been added to aid in fitting.

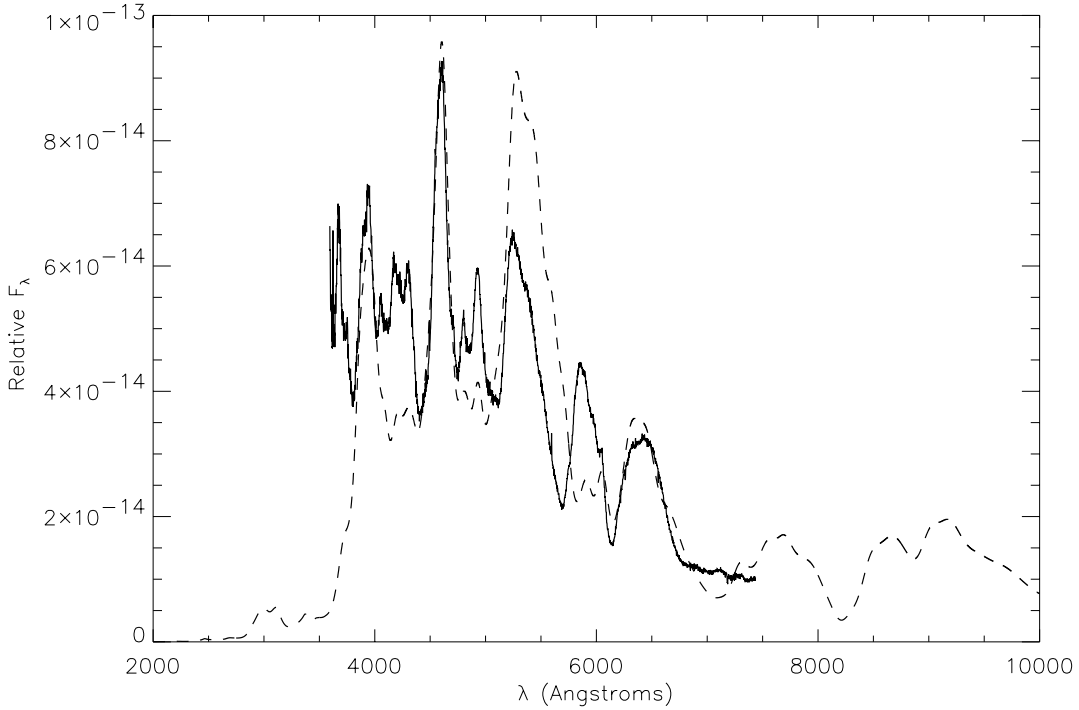


Fig. 17.— SN 1994D on 2 April 1994 (**?**, solid line,)]patat94D96 and W7 best fit synthetic spectrum for day 32 after explosion (dashed line).

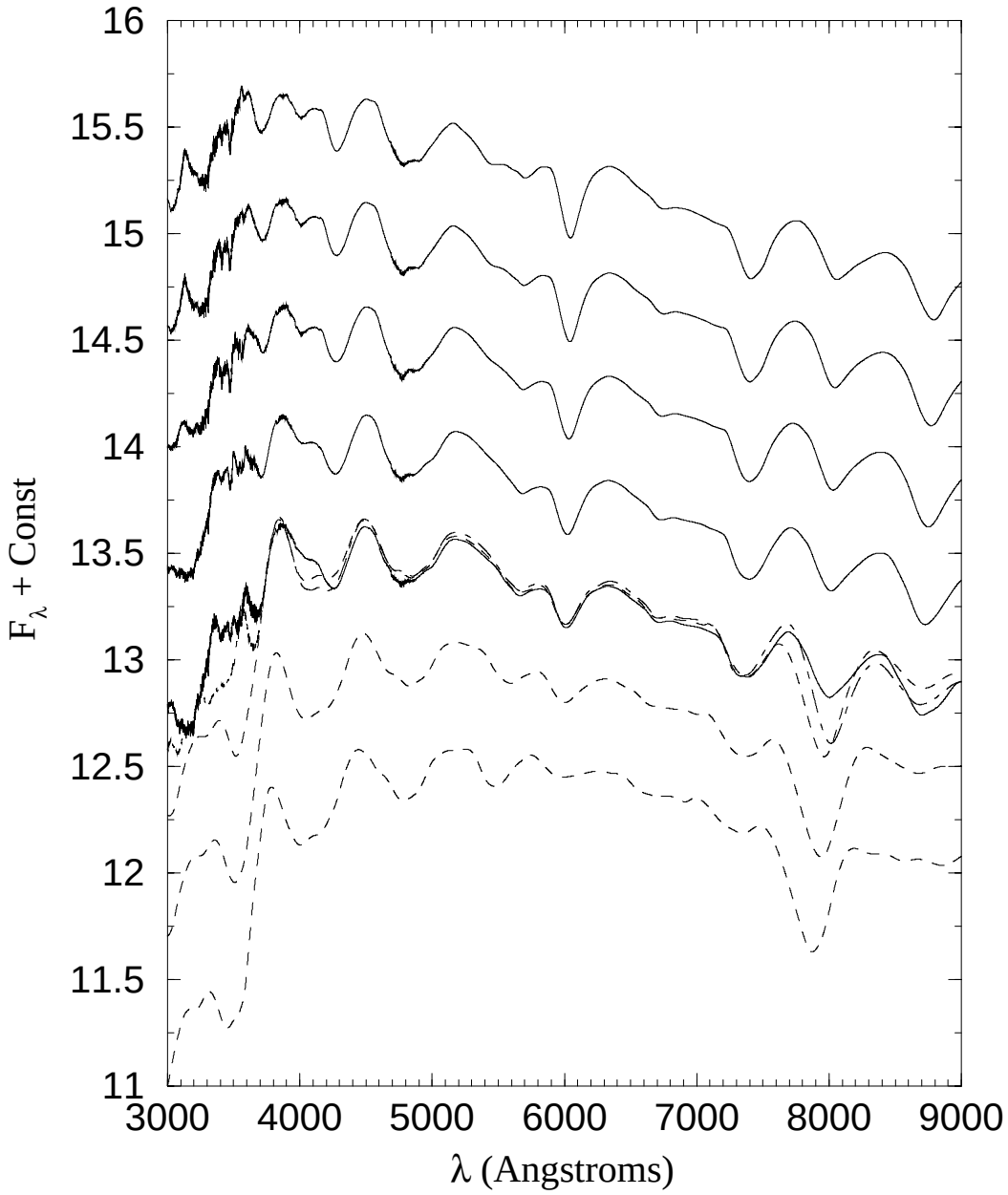


Fig. 18.— Synthetic spectra for the projected luminosities for days 1–7 (from bottom to top) after explosion. The dashed lines are the exponential models, and the dot-dashed line in day 3 is the exponential model that has been truncated at $v_{\rm max} = 30000$ km s$^{-1}$.

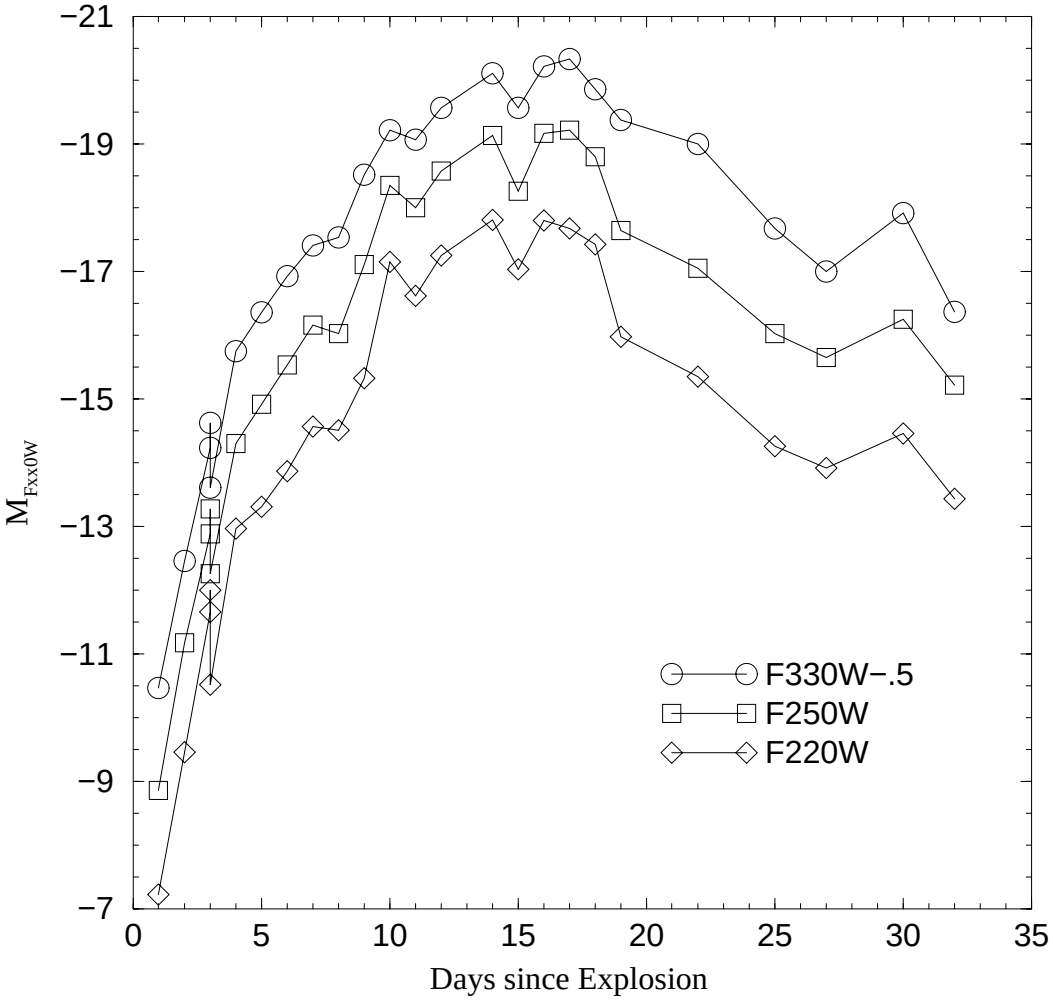


Fig. 19.— Ultra-violet synthetic photometry from the synthetic spectra. Arbitrary shifts in magnitude are noted in the legend in this and the following figures.

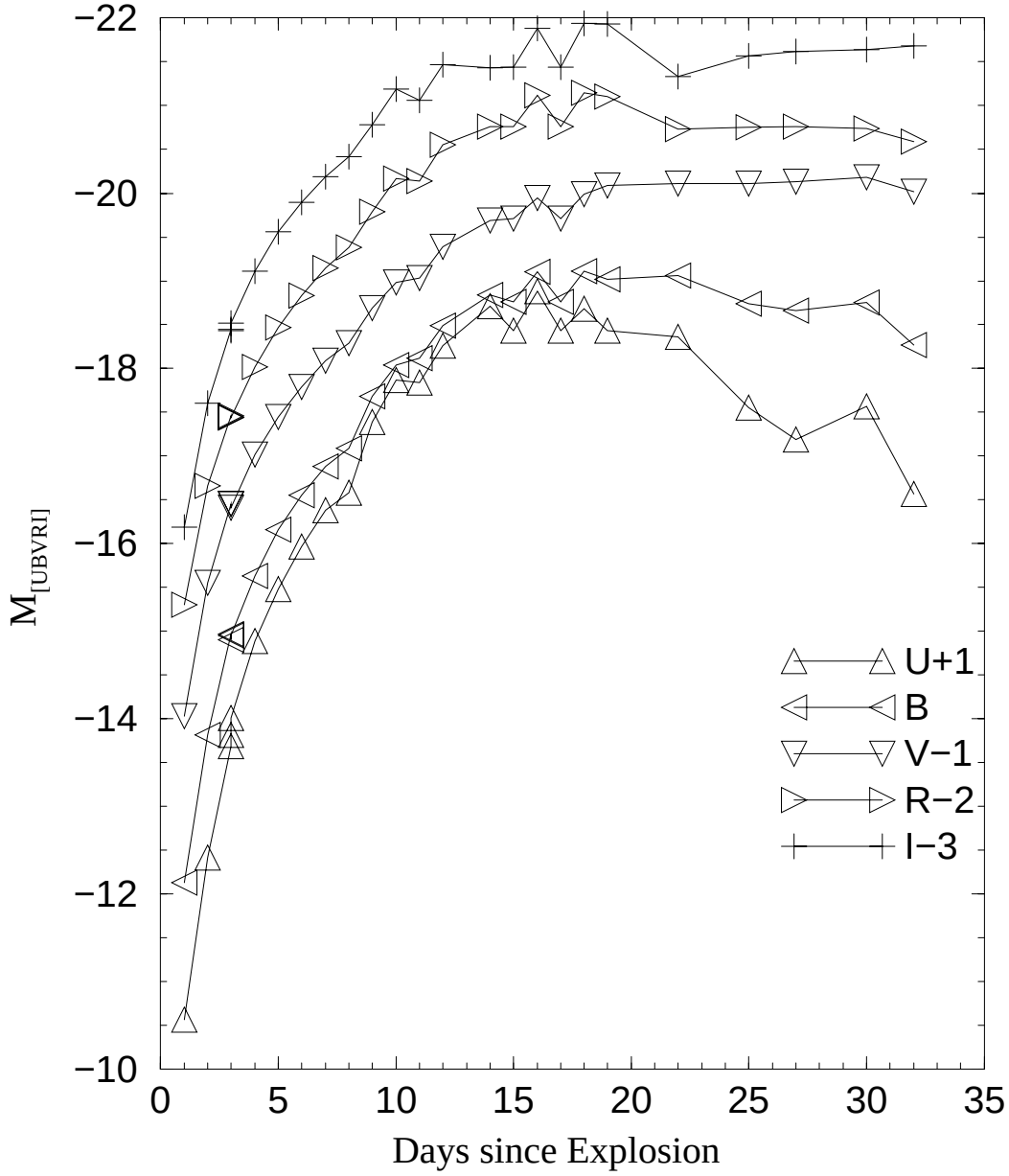


Fig. 20.— Synthetic optical/near-$IR$ photometry from the synthetic spectra.

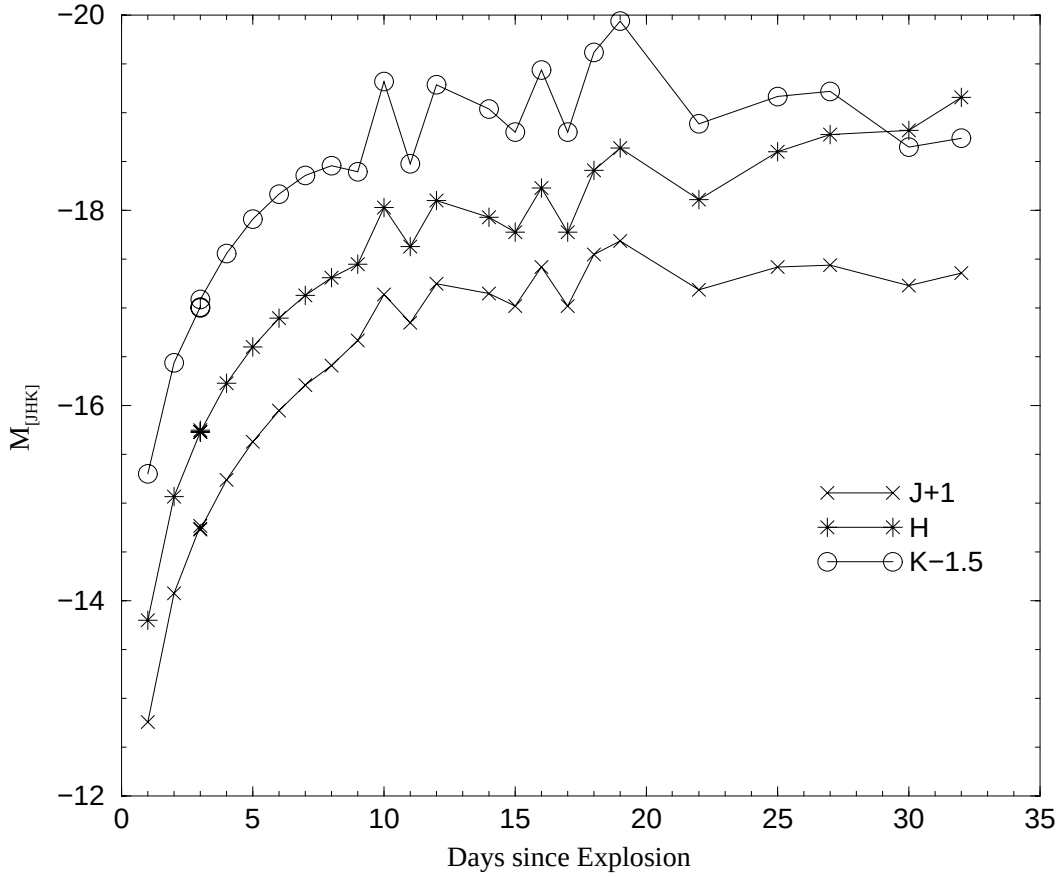


Fig. 21.— Infra-red synthetic photometry from the synthetic spectra.

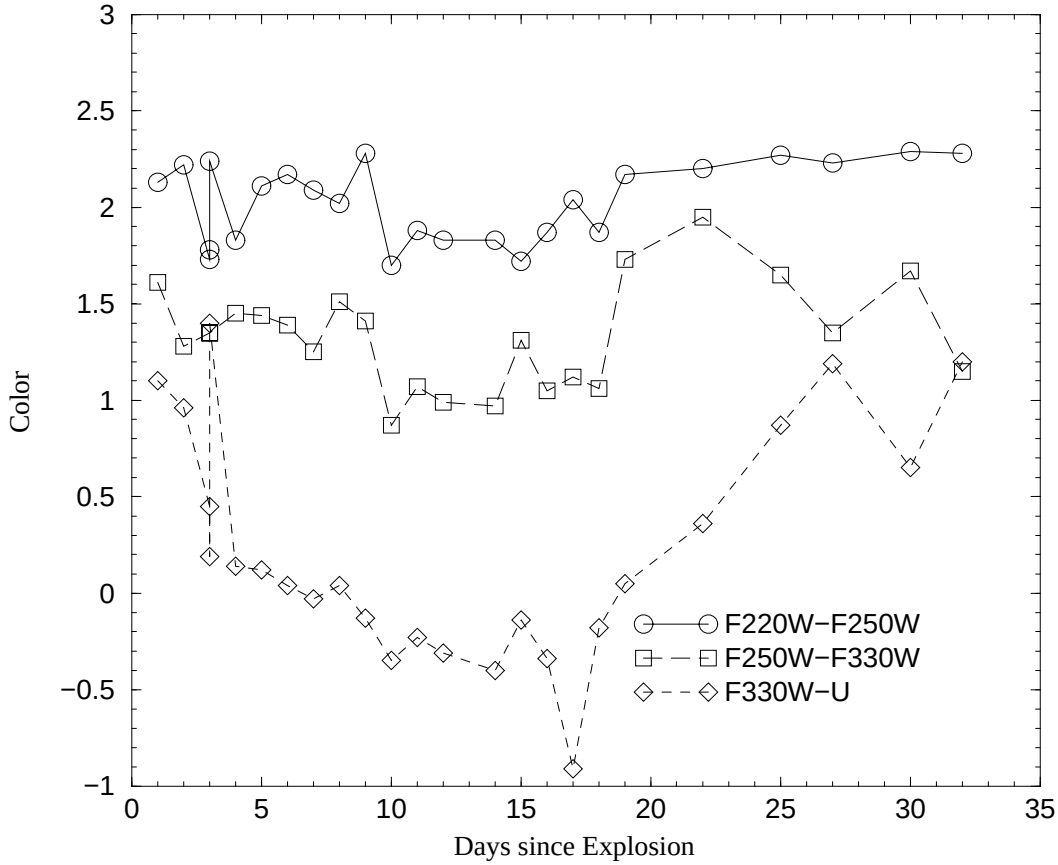


Fig. 22.— Ultra-violet synthetic colors from the synthetic spectra.

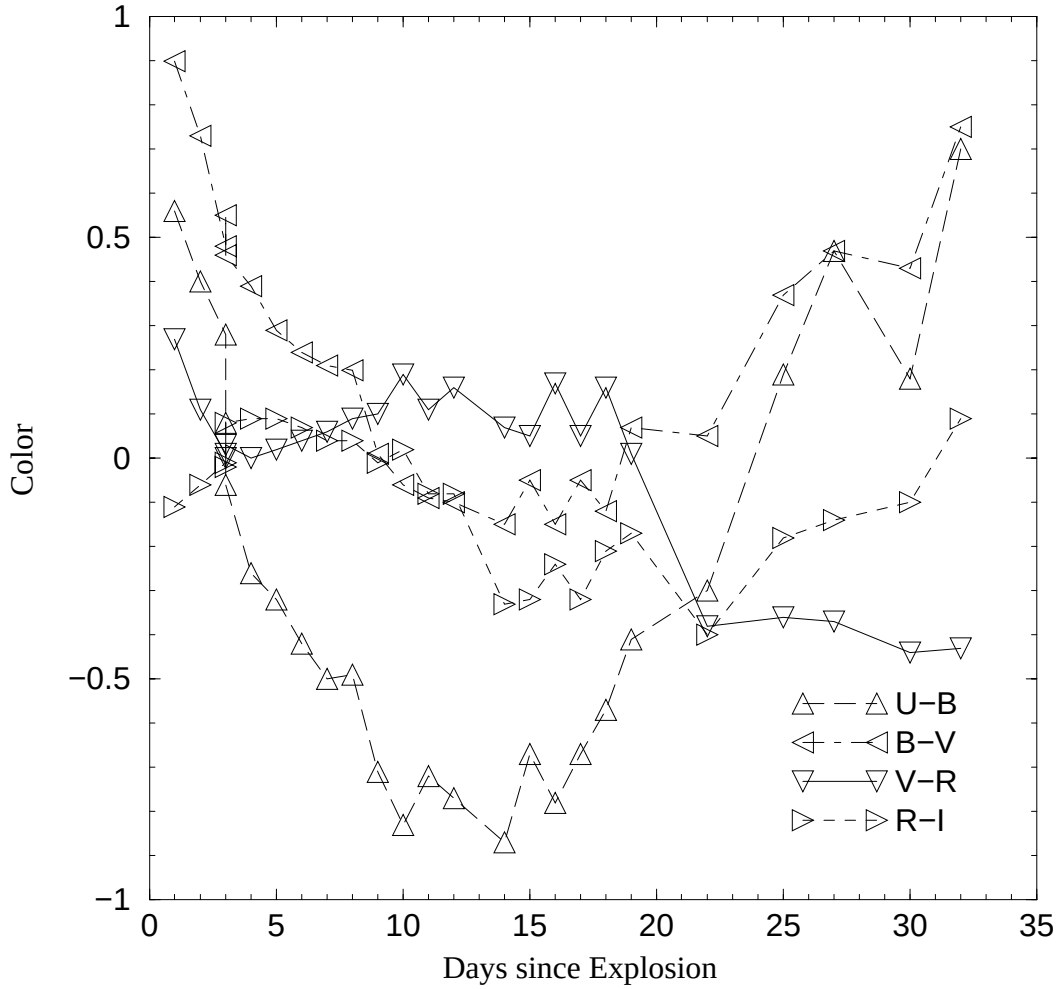


Fig. 23.— Synthetic colors from the synthetic spectra.

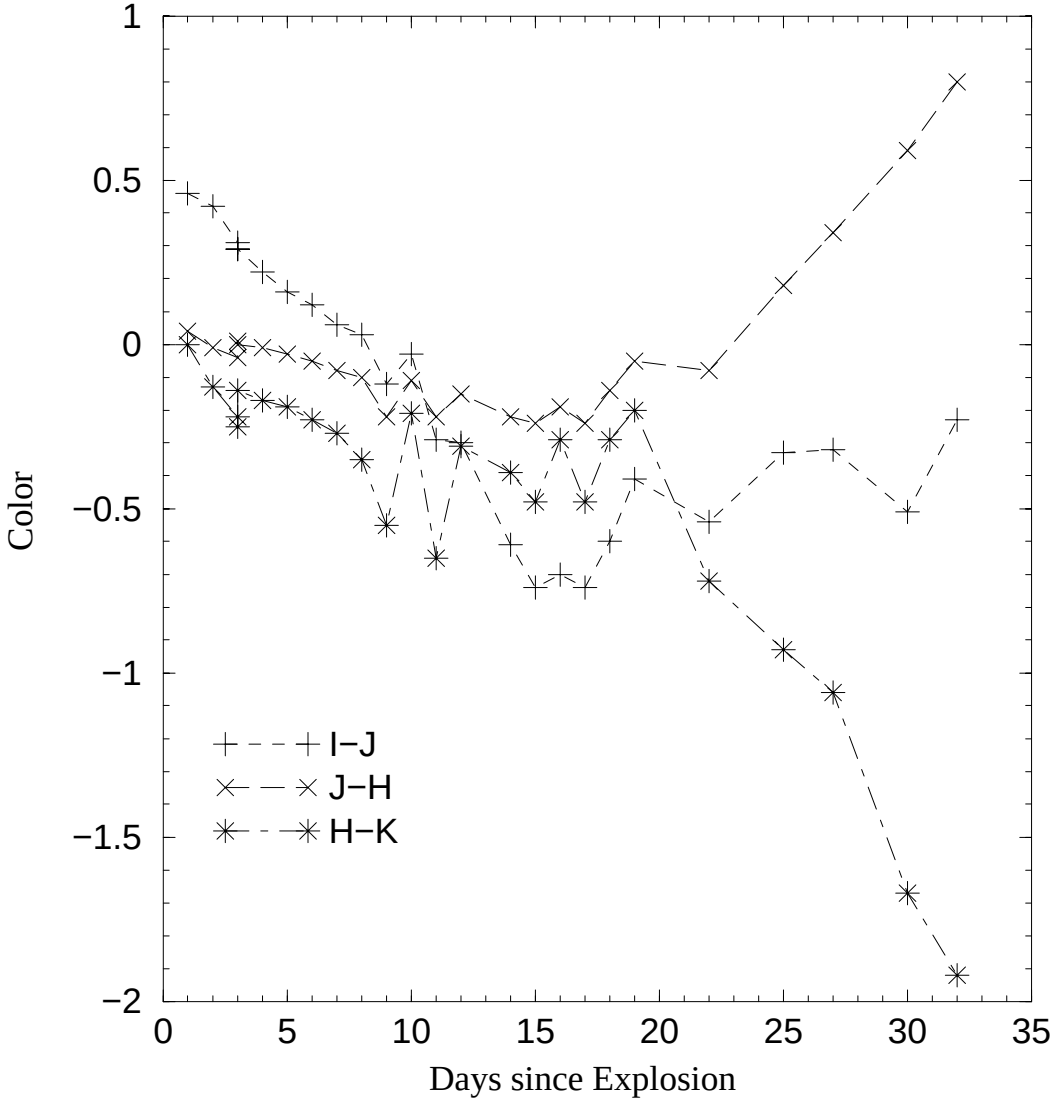


Fig. 24.— Infra-red synthetic colors from the synthetic spectra.

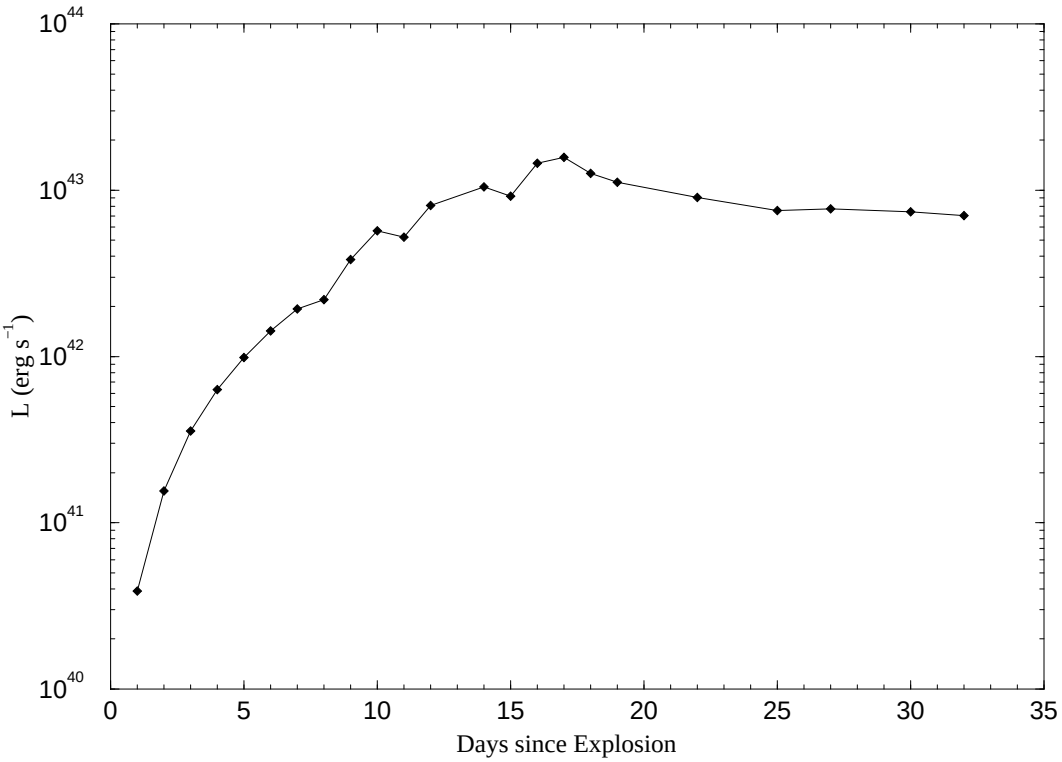


Fig. 25.— Bolometric light curve of synthetic spectra. The flatness of the bolometric light curve is likely due to the fact that the luminosity of the peak of W7 is too low because there was not enough mixing of $^{56}$Ni, which would force our fits to a larger luminosity at maximum (see § 3.1.11).

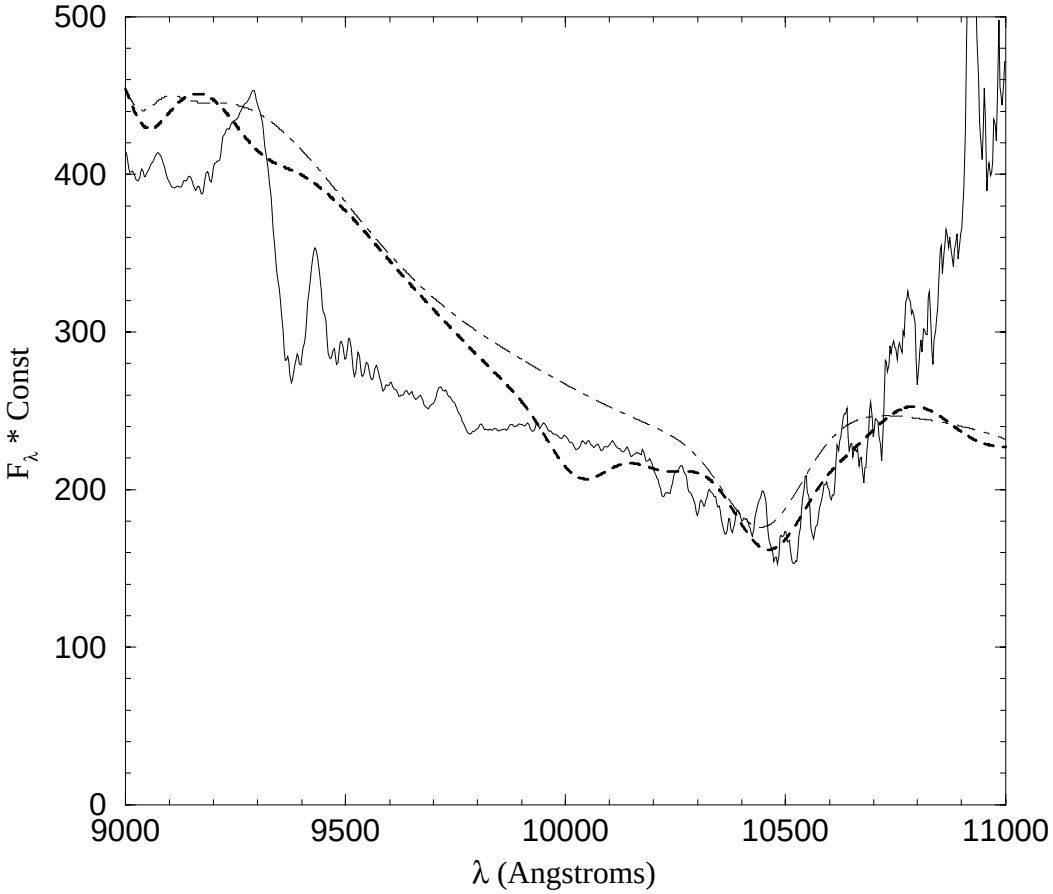


Fig. 26.— Near-$IR$ spectrum on 20 March 1994 (**?**, thin solid line)]patat94D96, best fit synthetic spectrum (thick dashed line), and best fit model using only Mg II line opacity. We believe that this firmly establishes the identity of this feature.

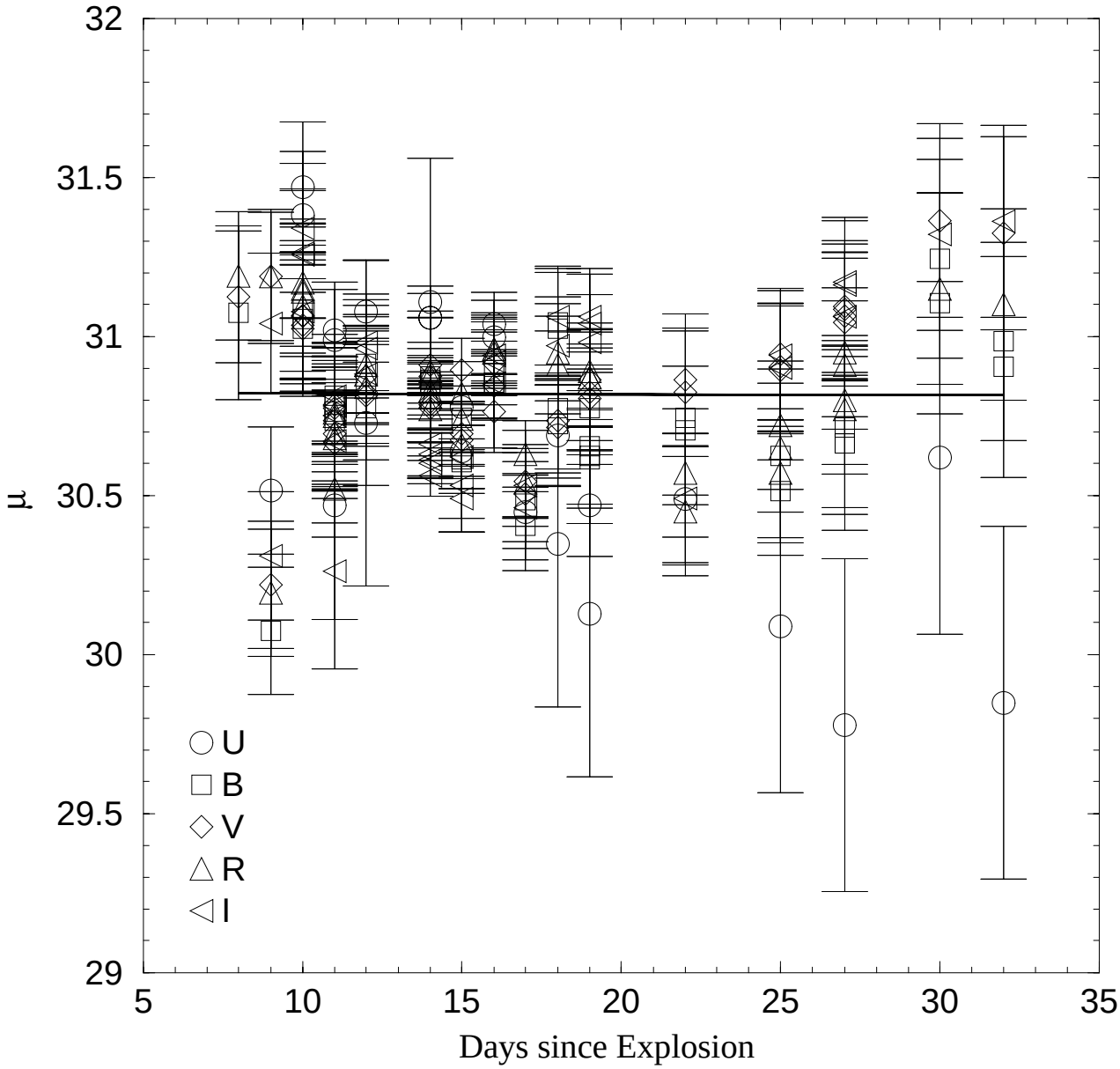


Fig. 27.— Distance moduli calculated from available observed photometry and associated photometry from synthetic spectra. The error bars combine the observers quoted errors and our estimate of the errors in our calculated luminosities. The solid line is a fit to the data which yields $\mu = 30.8 \pm 0.3$, consistent within errors with the results of Drenkhahn & Richtler (1999) and Höflich (1995).